Sequential Photosubstitution of Carbon Monoxide by *(E)*-Cyclooctene in Hexacarbonyltungsten: Structural Aspects, Multistep Photokinetics, and Quantum Yields

Friedrich-Wilhelm Grevels,* Jürgen Jacke, Werner E. Klotzbücher, Franz Mark,* Volker Skibbe, and Kurt Schaffner

Max-Planck-Institut für Strahlenchemie, Postfach 10 13 65, D-45413 Mülheim an der Ruhr, Germany

Klaus Angermund, Carl Krüger, and Christian W. Lehmann

Max-Planck-Institut für Kohlenforschung, Kaiser-Wilhelm-Platz 1, D-45470 Mülheim an der Ruhr, Germany

Saim Özkar*

Department of Chemistry, Middle East Technical University, 06531 Ankara, Turkey

Received April 23, 1999

The photochemical conversion of $W(CO)_6$ (**1**) into a *trans*-$W(CO)_4(\eta^2\text{-olefin})_2$ complex has been investigated using *(E)*-cyclooctene (eco) as a model olefin possessing extraordinary coordination properties. *trans*-$W(CO)_4(\eta^2\text{-eco})_2$ (**4**) is generated as an equimolar mixture of two diastereoisomers (**4a**, S_4 symmetry; **4b**, D_2 symmetry) which can be separated by fractional crystallization. The entire reaction sequence involves the intermediate formation of $W(CO)_5(\eta^2\text{-eco})$ (**2**) and *cis*-$W(CO)_4(\eta^2\text{-eco})_2$ (**3**: two diastereoisomers, **3a** and **3b**, with apparent C_s and C_2 symmetry, respectively). Complexes **2** and **3**, although difficult to isolate from the photochemical reaction mixture, are conveniently accessible via alternative thermal ligand exchange routes. The molecular structures of **2** and **4a** in the crystal were determined by X-ray diffraction techniques. The olefin double bonds, with *trans*-orthogonal arrangement in **4a**, are eclipsed to a OC−W−CO axis in either case. The course of the conversion of **1** into the olefin-substituted products was monitored by quantitative IR spectroscopy. Photokinetic equations developed for this study describe the concentrations of all four components as implicit functions of the amount of light absorbed by the system, of the quantum yields of the individual photoprocesses, and of the UV−vis absorbance coefficients of the compounds involved. Based on these functional relationships, the individual quantum yields at $\lambda_{exc} = 365$ nm ($\Phi_{12} = 0.73$, $\Phi_{23} = 0.34$, $\Phi_{24} = 0.16$, $\Phi_{34} = 0.15$) were evaluated from a series of experimental data sets by an iterative procedure which involves variation of the quantum yield input data until the best fit of the computed to the measured concentrations is achieved. Low-temperature matrix isolation techniques were employed to characterize the $W(CO)_4(\eta^2\text{-eco})$ fragment (**5**) as a key intermediate in the photolysis of $W(CO)_5(\eta^2\text{-eco})$ (**2**).

Introduction

Olefin-substituted group 6 metal carbonyls are conveniently accessible from the parent $M(CO)_6$ complexes (M = Cr, Mo, W) by means of photolytic CO detachment in the presence of the appropriate olefin. This has been demonstrated using ethene and linear alkenes,[1−5] cyclooalkenes,[5−7] α,β-unsaturated esters,[8] and tetracyanoethene[9] as the entering ligand. Upon continued irradiation, most of the initially generated $M(CO)_5(\eta^2\text{-olefin})$ complexes readily undergo secondary photosubstitution with formation of the respective *trans*-$M(CO)_4(\eta^2\text{-olefin})_2$ products. Apart from its synthetic potential, this chemistry may also be relevant to the carbonyltungsten-assisted isomerization of olefins.[10,11]

* To whom correspondence should be addressed. E-mail: grevels@mpi-muelheim.mpg.de.

(1) Stolz, I. W.; Dobson, G. R.; Sheline, R. K. *Inorg. Chem.* 1**963**, *2*, 1264−1267.
(2) Grevels, F.-W.; Jacke, J.; Özkar, S. *J. Am. Chem. Soc.* **1987**, *109*, 7536−7537.
(3) Gregory, M. F.; Jackson, S. A.; Poliakoff, M.; Turner, J. J. *J. Chem. Soc., Chem. Commun.* **1986**, 1175−1177.
(4) Banister, J. A.; Howdle, S. M.; Poliakoff, M. *J. Chem. Soc., Chem. Commun.* **1993**, 1814−1815.
(5) Jaroszewski, M.; Szymanska-Buzar, T.; Wilgocki, M.; Ziolkowski, J. J. *J. Organomet. Chem.* **1996**, *509*, 19−28.
(6) Grevels, F.-W.; Skibbe, V. *J. Chem. Soc., Chem. Commun.* **1984**, 681−683.
(7) Toma, J. M. D. R.; Toma, P. H.; Fanwick, P. E.; Bergstrom, D. E.; Byrn, S. R. *J. Crystallogr. Spectrosc. Res.* **1993**, *23*, 41−47.
(8) Grevels, F.-W.; Lindemann, M.; Benn, R.; Goddard, R.; Krüger, C. *Z. Naturforsch.* **1980**, *35b*, 1298−1309.
(9) (a) Herberhold, M. *Angew. Chem.* **1968**, *80*, 314−315; *Angew. Chem., Int. Ed. Engl.* **1968**, *7*, 305−306. (b) Mour, I. A.; Özkar, S. *Z. Naturforsch.* **1994**, *49b*, 717−720.

10.1021/om990300t CCC: $18.00
Publication on Web 07/24/1999

The existence of *cis*-$M(CO)_4(\eta^2$-olefin$)_2$ complexes and their possible involvement in the above photochemistry, along with the respective cis vacant $M(CO)_4(\eta^2$-olefin) fragments, has been addressed in theoretical studies,[12−14] and in photochemical experiments employing continuous irradiation at low temperatures in solid and liquid media,[3,5,15−17] and pulsed photolysis in the gas phase.[18,19] In this way, several *cis*-$M(CO)_4(\eta^2$-olefin$)_2$ complexes could indeed be detected and identified on the basis of some typical ν(CO) bands in the IR spectra, but no further characterization has been reported. The only member of this elusive class of compounds so far found to be sufficiently stable for isolation and comprehensive characterization is the one with *(E)*-cyclooctene (eco) as the olefin ligand, dealt with in this paper.[20] This cycloalkene is superior to other olefins with respect to its coordination ability. The particular stability of transition metal−eco bonds[21,22] apparently arises from substantial relief of ring strain upon complexation.[23] It also facilitates the study of the $M(CO)_5(\eta^2$-olefin)-type complex,[6,20] which commonly is, at best, moderately stable. Taking advantage of this property, we are now in a position to investigate the multistep photochemical conversion of $W(CO)_6$ (**1**) into a *trans*-$W(CO)_4(\eta^2$-olefin$)_2$ product (**4**) in full detail, including the evaluation of quantum yields for the individual steps in a complete photokinetic scheme with consideration of all mutual internal light filter effects.

Experimental Section

General Procedures. All reactions and manipulations were carried out under argon and in argon-saturated solvents, unless otherwise noted. Photochemical reactions on preparative scale were carried out in a water-cooled immersion-well apparatus[24] (solidex glass, $\lambda > 280$ nm) equipped with a Philips HPK 125-W high-pressure mercury lamp.

Spectra were recorded on the following instruments: NMR, Bruker ARX 250 (62.9 MHz for ^{13}C), Bruker WH 270 (270.1 MHz for ^{1}H, and 67.9 MHz for ^{13}C), and Bruker AM 400 (400.1 MHz for ^{1}H, and 100.6 MHz for ^{13}C); IR, Perkin-Elmer 1600 and Bruker IFS 66 (operating with 0.5 cm^{-1} for quantitative measurements); UV−vis, Bruins Instruments Omega 10. Elemental analyses were performed by Mikroanalytisches Laboratorium Dornis und Kolbe, Mülheim an der Ruhr.

Reagents. Analytical grade and deuterated solvents (Merck), *(Z)*-cyclooctene (zco; Merck), (+)-(1-phenyl)ethylamine (Fluka, chiraselect quality), and *(E,E)*-1,4-diphenyl-1,3-butadiene (Aldrich) were used as received.

(E)-Cyclooctene was prepared according to literature procedures[25,26] which were modified for large-scale production. (−)-*(E)*-Cyclooctene was separated from the racemic material via a platinum complex containing (+)-(1-phenyl)ethylamine, in analogy with a published procedure,[27] and extracted into *n*-hexane. The enantiomeric purity (≥99.5%) was checked by analytical GC (HP 5890 instrument, 30 m capillary column, 50 °C, 0.8 bar H_2 carrier gas) using a chiral stationary phase (Restek Rt-βDEXsa).

$W(CO)_6$ (**1**; Merck) was recrystallized from *n*-hexane [IR (*n*-hexane): ν(CO) 1983.3 cm^{-1} (ϵ = 73435 L·mol^{-1}·cm^{-1})]. $W(CO)_5(\eta^2$-*(Z)*-cyclooctene$)$[7,28] [pale yellow crystals, mp 90 °C (dec). IR (*n*-hexane): ν(CO) 2078.8 (m), 1960.1 (s), and 1946.6 (s) cm^{-1}. ^{1}H NMR (toluene-d_8): δ 3.91 (2 H), 2.24 (2 H), 1.59 (2 H), 1.23 (4 H), and 0.99 (4 H). ^{13}C NMR (toluene-d_8): δ 201.3 (s, CO_{ax}), 197.4 (s, CO_{eq}), 88.0 (d, $^1J_{CH}$ = 160 Hz; −CH═), 32.5 (t, $^1J_{CH}$ = 126 Hz; $-CH_2-$), 30.7 (t, $^1J_{CH}$ = 129 Hz; $-CH_2-$), and 25.9 (t, $^1J_{CH}$ = 125 Hz; $-CH_2-$)], $W(CO)_5[\eta^2$-bis(trimethylsilyl)ethyne$)]$,[29,30] and $W(CO)_4(\eta^4$-*(E,E)*-1,4-diphenyl-1,3-butadiene$)$[31] [orange crystals, purified by successive crystallization from toluene and *n*-pentane. IR (*n*-pentane): ν(CO) 2044.3 (m), 1973.1 (m), 1947.7 (s), and 1931.6 (s) cm^{-1}] were prepared according to the published procedures.

$W(CO)_5(\eta^2$-*(E)*-cyclooctene$)$ (2). A solution of *(E)*-cyclooctene (1.70 mL, 13.1 mmol) in *n*-hexane (10 mL) was added to solid $W(CO)_5(\eta^2$-*(Z)*-cyclooctene) (0.70 g, 1.61 mmol). The solution was stirred in the dark at room temperature for about 10 days (4 h at 60 °C gives the same result) until the starting material was no longer observed in the IR spectrum. Upon reducing the volume to ca. 2 mL and cooling the solution to −78 °C, pale yellow crystals of **2** precipitated (0.66 g, 94% yield); mp 69 °C (dec). IR (*n*-hexane): ν(CO) 2079.5 (3595), 1999.2 (vw), 1966.1 (20840), 1954.3 (9995), and 1947.4 cm^{-1} (ϵ = 22140 L·mol^{-1}·cm^{-1}). UV−vis (*n*-hexane): λ_{max} = 214 (41170), 239 (72160), 268 (8090), 302 (8780), and 353 nm (ϵ = 1340 L·mol^{-1}·cm^{-1}). ^{1}H NMR (toluene-d_8): δ 3.54 (2 H), 2.49 (2 H), 1.63 (4 H), 1.26 (2 H), 0.95 (2 H), 0.54 (2 H). ^{13}C NMR (toluene-d_8): δ 201.71 (s, CO_{ax}), 196.9 (s, CO_{eq}), 83.9 (d, $^1J_{CH}$ = 160 Hz; −CH═), 41.3 (t, $^1J_{CH}$ = 128 Hz; $-CH_2-$), 37.7 (t, $^1J_{CH}$ = 128 Hz; $-CH_2-$), 28.5 (t, $^1J_{CH}$ = 126 Hz; -CH_2-). Anal. Calcd for $C_{13}H_{14}O_5W$ (M = 434.1): C, 35.97; H, 3.25; W, 42.35. Found: C, 35.95; H, 3.50; W, 42.25.

***cis*-$W(CO)_4(\eta^2$-*(E)*-cyclooctene$)_2$ (3). Method A.** A solution of $W(CO)_5[\eta^2$-bis(trimethylsilyl)ethyne] (0.99 g, 2.0 mmol) and excess *(E)*-cyclooctene (1.10 g, 10 mmol) in *n*-hexane (100

(10) (a) Wrighton, M.; Hammond, G. S.; Gray, H. B. *J. Am. Chem. Soc.* **1970**, *92*, 6068−6070. (b) Wrighton, M.; Hammond, G. S.; Gray, H. B. *J. Am. Chem. Soc.* **1971**, *93*, 3285−3287. (c) Wrighton, M.; Hammond, G. S.; Gray, H. B. *J. Organomet. Chem.* **1974**, *70*, 283−301.
(11) Szymanska-Buzar, T.; Jaroszewski, M.; Wilgocki, M.; Ziólkowski, J. J. *J. Mol. Catal. A* **1996**, *112*, 203-210.
(12) Daniel, C.; Veillard, A. *Inorg. Chem.* **1989**, *28*, 1170−1173.
(13) Daniel, C.; Veillard, A. *Nouv. J. Chim.* **1986**, *10*, 83−90.
(14) Bachmann, C.; Demuynck, J.; Veillard, A. *J. Am. Chem. Soc.* **1978**, *100*, 2366−2369.
(15) Pope, K. R.; Wrighton, M. S. *Inorg. Chem.* **1985**, *24*, 2792−2796.
(16) Szymanska-Buzar, T.; Jaroszewski, M.; Downs, A. J.; Greene, T. M.; Morris, L. J. *J. Organomet. Chem.* **1997**, *531*, 207−216.
(17) Szymanska-Buzar, T.; Kern, K.; Stufkens, D. J. *New J. Chem.* **1998**, *22*, 1539−1544.
(18) Weiller, B. H.; Grant, E. R. *J. Am. Chem. Soc.* **1987**, *109*, 1252−1253.
(19) Takeda, H.; Jyo-o, M.; Ishikawa, Y.; Arai, S. *J. Phys. Chem.* **1995**, *99*, 4558−4565.
(20) Preliminary results have been communicated in: (a) Grevels, F.-W.; Jacke, J.; Klotzbücher, W. E.; Özkar, S.; Skibbe, V. *Pure Appl. Chem.* **1988**, *60*, 1017−1024. (b) Grevels, F.-W. In *Photoprocesses in Transition Metal Complexes, Biosystems and other Molecules. Experiments and Theory*; Kochanski, E., Ed.; Kluwer: Dordrecht, 1992; pp 141−171.
(21) Angermund, K.; Grevels, F.-W.; Krüger, C.; Skibbe, V. *Angew. Chem.* **1984**, *96*, 911−913; *Angew. Chem., Int. Ed. Engl.* **1984**, *23*, 904−905.
(22) (a) Ball, R. G.; Kiel, G.-Y.; Takats, J.; Krüger, C.; Raabe, E.; Grevels, F.-W.; Moser, R. *Organometallics* **1987**, *6*, 2260−2261. (b) Angermund, H.; Grevels, F.-W.; Moser, R.; Benn, R.; Krüger, C.; Romão, M. J. *Organometallics* **1988**, *7*, 1994−2004. (c) Angermund, H.; Bandyopadhyay, A. K.; Grevels, F.-W.; Mark, F. *J. Am. Chem. Soc.* **1989**, *111*, 4656−4661.
(23) Klassen, J. K.; Yang, G. K. *Organometallics* **1990**, *9*, 874−876.
(24) Grevels, F.-W.; Reuvers, J. G. A.; Takats, J. *Inorg. Synth.* **1986**, *24*, 176−180.
(25) Vedejs, E.; Snoble, K. A. J.; Fuchs, P. L. *J. Org. Chem.* **1973**, *38*, 1178−1183.
(26) Inoue, Y.; Tsuneishi, H.; Hakushi, T.; Tai, A. In *Photochemical Key Steps in Organic Synthesis, an Experimental Course Book*; Mattay, J., Griesbeck, A., Eds.; VCH: Weinheim, 1994; p 207.
(27) Cope, A. C.; Ganellin, C. R.; Johnson, H. W., Jr.; Van Auken, T. V.; Winkler, H. J. S. *J. Am. Chem. Soc.* **1963**, *85*, 3276−3279.
(28) Skibbe, V. Doctoral Dissertation; Universität Duisburg/MPI für Strahlenchemie, 1985.
(29) Jacke, J. Doctoral Dissertation; Universität Duisburg/MPI für Strahlenchemie, 1989.
(30) Grevels, F.-W.; Jacke, J.; Krüger, C. Manuscript in preparation.
(31) Özkar, S.; Peynircioglu, N. B. *Inorg. Chim. Acta* **1986**, *119*, 127−129.

mL) was stirred for 24 h at ambient temperature in the dark. After reducing the volume to 50 mL the solution was cooled to dry ice temperature, whereupon yellow crystals of **3** precipitated (0.46 g, 45%); a second crop (0.17 g, 16%) was obtained after reducing the volume of the mother liquor to 10 mL. The isolated samples are mixtures of two isomers, **3a** (major component) and **3b**, as identified by ^{13}C NMR spectroscopy. IR (*n*-hexane): ν(CO) ~2037 (s), ~1950 (vs), ~1934 (vs), ~1930 (m, sh), ~1914 (w), ~1894 (m) cm^{-1}. UV−vis (*n*-hexane): λ_{max} = 245 (42600), 288 (12900), 325 nm (sh, ϵ = 7300 L·mol^{-1}·cm^{-1}). ^{1}H NMR (benzene-d_6): δ 3.47/3.42 (4 H), 2.56 (4 H), 1.61−1.78 (8 H), 1.03−1.44 (8H), 0.45−0.76 (4 H). ^{13}C NMR (toluene-d_8, 253 K): (**3a**) δ 206.83 (CO_{eq}), 201.55 (CO_{ax}), 201.33 (CO_{ax}), 81.63 (−CH═), 40.17 (−CH_2−), 37.59 (−CH_2−), 28.60 (−CH_2−); (**3b**) δ 208.28 (s, CO_{eq}), 204.95 (s, CO_{ax}), 86.69 (−CH═), 39.68 (−CH_2−), 37.33 (−CH_2−), 28.43 (−CH_2−). Anal. Calcd for $C_{20}H_{28}O_4W$ (M = 516.4): C, 46.53; H, 5.47; W, 35.61. Found: C, 46.48; H, 5.60; W, 35.29.

Method B. A solution of W(CO)$_4$(η^4-*(E,E)*-1,4-diphenyl-1,3-butadiene) (0.05 g, 0.1 mmol) and *(E)*-cyclooctene (0.07 mL, 0.5 mmol) in *n*-hexane (5 mL) was stirred at ambient temperature in the dark, whereupon the solution changed its color from orange to yellow. Quantitative conversion into **3** occurs within 30 min, as monitored by IR spectroscopy. After removal of *(E,E)*-1,4-diphenyl-1,3-butadiene, which precipitated upon cooling the solution to −40 °C, yellow crystals of **3** (ratio **3a**:**3b** ≈ 1:1, by ^{13}C NMR) were isolated at −78 °C.

The analogous reaction of W(CO)$_4$(η^4-*(E,E)*-1,4-diphenyl-1,3-butadiene) (1.5 mM) with (−)-*(E)*-cyclooctene (10-fold excess) in *n*-hexane was monitored by means of quantitative IR spectroscopy in order to record the ν(CO) pattern of *cis*-W(CO)$_4$-[η^2-(−)-eco]$_2$ (**3b″**), which is one of the enantiomers of **3b**: 2035.8 (4885), 1948.6 (13460), 1930.7 (2600), 1914.2 (2515), and 1894.1 cm^{-1} (ϵ = 6505 L·mol^{-1}·cm^{-1}).

Computer-assisted subtraction of the **3b″** spectrum from quantitative spectra of **3a**+**3b** mixtures, generated from W(CO)$_4$(η^4-*(E,E)*-1,4-diphenyl-1,3-butadiene) (1.5 mM) and racemic *(E)*-cyclooctene (10-fold excess), yielded the ν(CO) pattern of **3a**: 2037.3 (4930), 1950.0 (1760), 1933.4 (ϵ = 19315 L·mol^{-1}·cm^{-1}), and 1929 (sh) cm^{-1}. The **3a**:**3b** ratio in such solutions was found to change with time from ca. 50:50 (initial ratio) to ca. 75:25 (equilibrium ratio), while the total concentration remained constant.

***trans*-W(CO)$_4$(η^2-*(E)*-cyclooctene)$_2$ (4).** A solution of W(CO)$_6$ (**1**; 1.06 g, 3.00 mmol) and *(E)*-cyclooctene (2.8 mL, 22 mmol) in *n*-pentane (300 mL) was irradiated while a stream of argon was passed through the solution. The irradiation was continued until the IR bands of **1** and of the intermediate products **2** and **3** had largely disappeared (2 h). The slightly turbid solution was filtered and evaporated to dryness in vacuo. The residue was an equimolar mixture of two isomeric products, **4a** and **4b**, as recognized by ^{13}C{^{1}H} NMR spectroscopy. Recrystallization from toluene (35 mL; dissolved at 20 °C, cooled to −25 °C) yielded colorless crystals of pure **4a** (0.52 g, 34%; mp 192−195 °C, dec, sealed capillary). After reducing to 15 mL the mother liquor was cooled to −78 °C, whereupon colorless crystals of **4a**+**4b** (70:30 ratio, by ^{13}C{^{1}H} NMR; 0.21 g, 14%) precipitated. After removal of toluene from the remaining solution, the remnant was dissolved in *n*-hexane and filtered over silica gel. Crystallization from *n*-hexane (15 mL; dissolved at 20 °C, cooled to −78 °C) yielded colorless crystals of pure **4b** (0.53 g, 34%; mp 176 °C, dec, sealed capillary). IR (*n*-hexane; the spectra of **4a** and **4b** are virtually identical): ν(CO) 1983.8 (vw) and 1949.9 cm^{-1} (ϵ = 34450 L·mol^{-1}·cm^{-1}). UV−vis (*n*-hexane, the spectra of **4a** and **4b** are virtually identical): λ_{max} = 243 (53560) and 293 nm (ϵ = 2560 L·mol^{-1}·cm^{-1}). ^{1}H NMR (toluene-d_8): **(4a)** δ 2.64 (4 H), 2.57 (4 H), 1.83 (8 H), 1.44 (4 H), and 0.99 (8 H). ^{13}C/^{13}C{^{1}H} NMR (toluene-d_8): **(4a)** δ 200.93 (s, CO), 57.76 (d, $^1J_{CH}$ = 151 Hz; −CH═), 41.94 (t, $^1J_{CH}$ = 125 Hz; −CH_2−), 38.24 (t, $^1J_{CH}$ = 128 Hz; −CH_2−), and 29.14 (t, $^1J_{CH}$ = 124 Hz; −CH_2−); **(4b)** δ 200.88 (s and d, $^1J_{CW}$ = 123 Hz, CO), 58.05 (s and d, $^1J_{CW}$ = 14 Hz, −CH═), 41.85 (−CH_2−), 38.28 (−CH_2−), and 29.16 (−CH_2−). MS (the spectra of **4a** and **4b** are virtually identical): m/z = 516 (M$^+$), 488 and other fragment ions. Anal. Calcd for $C_{20}H_{28}O_4W$: C, 46.53; H, 5.47; W, 35.61. Found: (**4a**) C, 46.78; H, 5.13; W, 35.84.

Quantum Yields. Light absorption was measured by means of a modified version of an electronically integrating actinometry device,[32] which compensates for incomplete absorption of light in the sample cell. The instrument was calibrated by ferrioxalate actinometry.[33] Irradiation at 365 nm of 3.0 mL aliquots of stock solutions of complexes **1** (ca. 1.5 mM), **2** (ca. 1.5 mM), or **3** [ca. 1.3 mM, ratio **3a**:**3b** ≈ 3:1, generated by method B from W(CO)$_4$(η^4-*(E,E)*-1,4-diphenyl-1,3-butadiene) and *(E)*-cyclooctene] in *n*-hexane containing *(E)*-cyclooctene (≥10-fold excess) was carried out at 25 ± 1 °C in quartz cuvettes (d = 1 cm) by using a Hanovia 1000 W Hg−Xe lamp connected to a Schoeffel Instruments GM 252 grating monochromator. The light intensity at 365 nm was on the order of 2 × 10^{-6} einstein·min^{-1} absorbed by the 3.0 mL samples.

Quantitative IR spectroscopy (Bruker IFS 66 spectrometer operating with 0.5 cm^{-1} resolution; IR cell with CaF_2 windows, d = 509 μm), with computer-assisted subtraction of spectra, was employed to determine the concentrations of the involved carbonyltungsten complexes on the basis of the ν(CO) absorbance data reported above. The study includes 10 individual runs starting with **1** (with conversions up to 80%; cf. Figure 9),[34] 12 individual runs starting with **2** (with conversions up to 70%; cf. Figure 8),[34] and 8 individual runs starting with **3** (with conversions up to 50%; cf. Figure 4).[34] The following UV−vis molar absorbance data at 365 nm were used to account for mutual internal light filtering. **1**: ϵ = 305 L·mol^{-1}·cm^{-1}. **2**: ϵ = 1010 L·mol^{-1}·cm^{-1}. **3**: ϵ = 1540 L·mol^{-1}·cm^{-1}. **4**: ϵ = 170 L·mol^{-1}·cm^{-1}.

Low-Temperature Matrix Photochemistry. The equipment has been described previously,[35] including the devices for controlling the temperature (10−12 K), flow of matrix gas (1.5−2 mmol·h^{-1}), and metal complex deposition rate, the setup for monochromatic and broad-band irradiation, and the IR (Perkin-Elmer 580) and UV−vis (Perkin-Elmer 320) spectrometers. The evaporation temperature (29 °C) of complex **2** was adjusted (quartz microbalance) to achieve a guest/host ratio of ≤1:1000.

X-ray Diffraction Structure Analyses. Crystals of **2** and **4a**, recrystallized from *n*-pentane, were mounted in glass capillaries under argon. Details of the X-ray crystal structure analyses are given in Table 1. The structures were solved by the heavy atom method (SHELXS-86).[36] Refinement was by full matrix least-squares methods (GFMLX highly modified version of ORFLS),[37] where the function $\sum w(\Delta F)^2$ was minimized with $w = 1/\sigma(F)^2$ and $\Delta F = |F_o| - |F_c|$ for **4a** and SHELXL-97 where the function $\sum w(F_o^2 - F_c^2)^2$ was minimized for **2**. H atom positions were found and included but constrained in the final refinement stage for both compounds.

(32) Amrein, W.; Gloor, J.; Schaffner, K. *Chimia* **1974**, *28*, 185−188.

(33) (a) Hatchard, C. G.; Parker, C. A. *Proc. R. Soc. London A* **1956**, *235*, 518−536. (b) Murov, S. L. *Handbook of Photochemistry*; Dekker: New York, 1973; p 119.

(34) The concentrations and the amount of absorbed light are normalized to the initial concentration of the starting material **1** (Figure 9), **2** (Figure 8), or **3** (Figure 4) by setting $\tilde{c}_i = c_i/c^0_{1(or2)(or3)}$ and $\tau = (1/c^0_{1(or2)(or3)})\int^t_0 Q_{abs}\,dt$.

(35) (a) Gerhartz, W.; Grevels, F.-W.; Klotzbücher, W. E. *Organometallics* **1987**, *6*, 1850−1856. (b) Klotzbücher, W. E. *Cryogenics* **1983**, *23*, 554−556.

(36) Sheldrick, G. M. *Acta Crystallogr. A* **1990**, *46*, 467−473.

(37) Busing, W. R.; Martin, K. O.; Levy, H. A. *ORFLS, Report ORNL-TM-305*; Oak Ridge National Laboratory: TN, 1962.

Table 1. Details of the X-ray Crystal Structure Analyses for the Complexes 2 and 4a

	2	**4a**
formula	$C_{13}H_{14}O_5W$	$C_{20}H_{28}O_4W$
mol wt, g·mol^{-1}	434.1	516.3
cryst color	pale yellow	colorless
cryst syst	monoclinic	monoclinic
space group [no.]	$P2_1/c$ [14]	$C2/c$ [15]
a, Å	12.3481(8)	13.460(2)
b, Å	8.3768(5)	14.382(2)
c, Å	13.4821(9)	12.412(2)
β, deg	95.469(2)	122.50(1)
V, Å^3	1388.21(15)	2026.6
Z	4	4
D_{calcd}, g·cm^{-3}	2.077	1.69
μ, cm^{-1}	83.33	58.4
Mo Kα radiation, λ, Å	0.71073	0.71069
$F(000)$, e	824	1016
diffractometer	Siemens Smart-CCD	Enraf-Nonius CAD4
scan mode	ω	$\omega-2\theta$
$[(\sin\theta)/\lambda]_{max}$, Å^{-1}	0.70	0.70
T, K	100	293
cryst size, mm	0.13 × 0.10 × 0.06	
abs corr	empirical	empirical
(min., max.)	0.57, 0.93	0.859, 1.404
no. of measd reflcns	12089 ($\pm h$, $\pm k$, $+l$)	5853 ($\pm h$, $\pm k$, $+l$)
no. of indep reflcns	4763	2984
no. of obsd reflcns ($I > 2\sigma(I)$)	3610	2491
R_{av}	0.04	0.02
no. of refined params	172	109
R_1	0.0355	0.024
wR^2/R_w [$w = 1/\sigma^2(F_o)$]	0.0799	0.024
resid electron dens, e Å^{-3}	2.371	0.66

Table 2. Selected Bond Lengths (Å) and Angles (deg) for W(CO)$_5$(η^2-eco) (2) and *trans*-W(CO)$_4$(η^2-eco)$_2$ (4) (Isomer 4a)

2		**4a**	
	Bond Lengths[a]		
W−C(1)	2.047(5)	W−C(1)	2.026(5)
W−C(2)	2.069(5)		
W−C(3)	2.050(5)	W−C(2)	2.049(4)
W−C(4)	2.031(4)		
W−C(5)	2.011(5)		
O(1)−C(1)	1.141(6)	O(1)−C(1)	1.150(6)
O(2)−C(2)	1.136(6)		
O(3)−C(3)	1.134(6)	O(2)−C(2)	1.134(6)
O(4)−C(4)	1.148(6)		
O(5)−C(5)	1.150(6)		
W−C(11)	2.451(5)	W−C(22)	2.328(3)
W−C(12)	2.425(4)		
		W−C(12)	2.327(3)
C(11)−C(12)	1.384(6)	C(22)−C(22)*	1.412(6)
		C(12)−C(12)*	1.424(5)
	Bond and Torsional Angles[a]		
C(12)−W−C(11)	33.0(2)	C(22)*−W−C(22)	35.3(1)
		C(12)*−W−C(12)	35.6(1)
C(18)−C(11)−C(12)−C(13)	−131.4	C(13)*−C(12)*−C(12)−C(13)	123.7
		C(23)−C(22)−C(22)*−C(23)*	123.4
C(2)−W−C(11)−C(12)	92.5	C(22)*−C(22)−W−C(2)	86.1
C(1)−W−C(11)−C(12)	−89.7	C(12)*−C(12)−W−C(1)	91.7
C(4)−W−C(11)−C(12)	0.0	C(22)*−C(22)−W−C(1)	175.2
C(3)−W−C(11)−C(12)	180.0	C(2)−W−C(12)−C(12)*	178.7
		Plane(1)[b]−Plane(2)[b]	87.7
O(1)−C(1)−W	179.3(4)	O(2)−C(2)−W	177.9(3)
O(2)−C(2)−W	177.6(4)	O(1)−C(1)−W	176.8(3)
O(3)−C(3)−W	178.4(4)		
O(4)−C(4)−W	178.1(4)		
O(5)−C(5)−W	176.5(4)		
C(2)−W−C(1)	177.0(2)	C(1)*−W−C(1)	176.6(1)
C(3)−W−C(4)	175.4(2)	C(2)*−W−C(2)	176.2(1)
C(3)−W−C(2)	88.3(2)	C(2)*−W−C(1)	91.2(2)
C(4)−W−C(2)	92.8(2)	C(2)−W-C(1)	88.9(2)
C(5)−W−C(2)	91.1(2)		
C(5)−W−C(3)	90.1(2)		

[a] Esd's are given in parentheses. [b] Plane(1) = W−C(12)−C(12)*, Plane(2) = W−C(22)−C(22)*.

ORTEP drawings[38] of the molecular structures are displayed in Figure 1 (complex **4a**) and Figure 5 (complex **2**), and selected bond distances and angles are collectively listed in Table 2. More comprehensive collections of structure data and complete lists of atomic coordinates and thermal parameters are available as Supporting Information for **2** (Tables S-1, S-2, S-3) and **4a** (Tables S-4, S-5, S-6). X-ray diffraction studies of W(CO)$_6$[39]

(38) Johnson, C. K. *ORTEP II, Report ORNL-5138*; Oak Ridge National Laboratory: TN, 1976.

Scheme 1

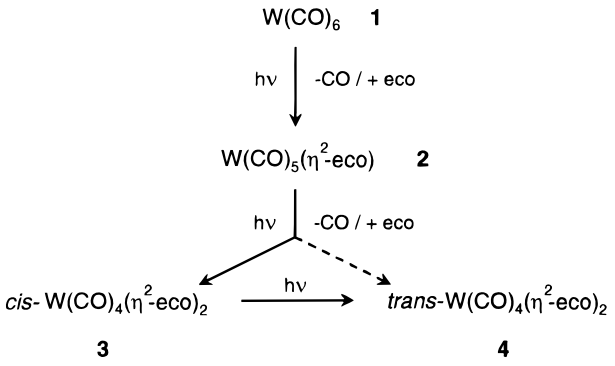

and *trans*-W(CO)$_4$(η^2-zco)$_2$[40] were carried out in connection with the work described in this paper and, independently, by other authors[7,41] as well. Our results (bond lengths and angles, atomic coordinates, and thermal parameters) are available as Supporting Information for W(CO)$_6$ (**1**) (Figure S-1; Tables S-7, S-8, S-9) and *trans*-W(CO)$_4$(η^2-zco)$_2$ (Figure S-2; Tables S-10, S-11, S-12).

Results and Discussion

The photochemical conversion of W(CO)$_6$ (**1**) in the presence of excess *(E)*-cyclooctene (eco) into *trans*-W(CO)$_4$(η^2-eco)$_2$ (**4**), monitored by IR spectroscopy (vide infra), involves two intermediate products, which are identified as W(CO)$_5$(η^2-eco) (**2**) and *cis*-W(CO)$_4$(η^2-eco)$_2$ (**3**) (Scheme 1). Although difficult to isolate from the photochemical reaction mixtures at any stage of the conversion, compounds **2** and **3** are conveniently accessible via alternative thermal ligand exchange routes.

***trans*-Tetracarbonylbis(η^2-*(E)*-cyclooctene)tungsten (4).** Extended irradiation of **1** in the presence of *(E)*-cyclooctene ultimately results in the nearly complete conversion into *trans*-W(CO)$_4$(η^2-eco)$_2$ (**4**) (Scheme 1). The appearance of one single strong ν(CO) band in the IR spectrum of **4** is indicative of a square-planar structure of the W(CO)$_4$ skeleton, which implies that in the presumed octahedral coordination geometry the olefin ligands are in mutual trans-positions.

In general, bis-olefin complexes can exist in different diastereoisomeric forms if the olefin is prochiral (two enantiotopic sites) or chiral. Accordingly, two diastereoisomers of complex **4** are expected from the reaction of **1** with racemic *(E)*-cyclooctene. One of them, **4a**, contains both enantiomers of *(E)*-cyclooctene in the same complex molecule, while the other one, **4b**, is a racemate of two enantiomeric complexes each carrying two molecules of the same *(E)*-cyclooctene enantiomer.

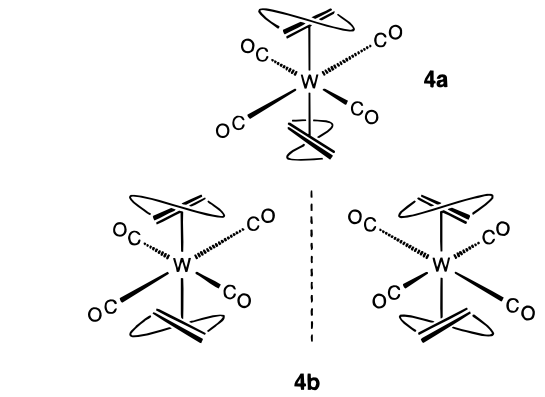

The crude product is indeed a nearly equimolar mixture of two isomers which were separated from each other by fractional crystallization with a total yield on the order of 80%. The two isomers give virtually identical ν(CO) spectra, but are clearly distinguishable by ^{13}C NMR spectroscopy. However, a definite assignment is not possible on this basis, since they both exhibit the same number of resonances, namely, one line in the carbonyl region and four signals for the *(E)*-cyclooctene ligand.

X-ray crystallography reveals (Figure 1) that the less soluble isomer has the structure **4a** (S_4 molecular symmetry), which leaves structure **4b** (D_2 molecular symmetry) for the other isomer. The trans-orthogonal orientation of the two olefins, eclipsed to the respective OC−W−CO axes of the square-planar W(CO)$_4$ moiety, is in accord with theoretical predictions made for the related complex *trans*-Mo(CO)$_4$(η^2-ethene)$_2$[14] and was also observed for the analogous complex of *(Z)*-cyclooctene, *trans*-W(CO)$_4$(η^2-zco)$_2$.[7,40] In the latter compound the W−C(olefin) distances are slightly longer, by ca. 0.03 Å, than those in **4a** (Table 2), thus underlining the better coordination ability of *(E)*-cyclooctene.

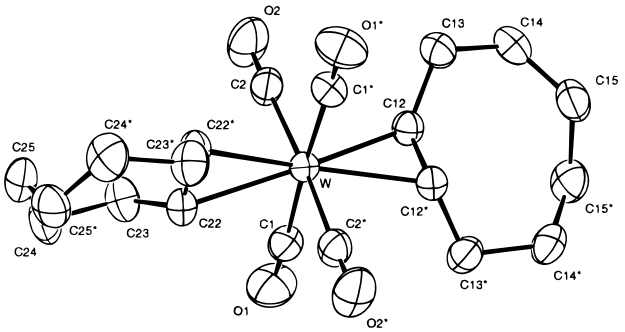

Figure 1. Structure of *trans*-W(CO)$_4$(η^2-eco)$_2$ (isomer **4a**, S_4 symmetry) in the crystal.

(39) Crystal data of W(CO)$_6$ (**1**): C_6O_6W, colorless crystals, molecular weight 351.9 g·mol^{-1}, crystal size 0.13 × 0.29 × 0.36 mm, a = 11.965(3) Å, b = 11.392(4) Å, c = 6.465(1) Å, V = 881.3(3) Å^3, T = 293 K, d_{calc} = 2.65 g·cm^{-3}, μ = 133.81 cm^{-1}, Z = 4, orthorhombic, space group *Pnma* (no. 62), Enraf-Nonius-CAD4 diffractometer, $\omega-2\theta$ scan mode, λ = 0.71069 Å, empirical absorption correction (min. 0.777, max. 1.288), 10522 measured reflections ($\pm h,\pm k,\pm l$), $[(\sin\theta)/\lambda]_{max}$ 0.70 Å^{-1}, 1322 independent and 1012 observed reflections [$I \geq 2\sigma(I)$], 67 refined parameters, heavy atom method, R_1 = 0.027, R_w = 0.035 [$w = 1/\sigma^2(F_o)$], residual electron density 1.69 e Å^{-3}. The molecular structure in the crystal is essentially octahedral, although slightly differing W−C (2.020−2.055 Å) and C−O distances (1.14−1.16 Å) are found.

(40) Crystal data of *trans*-W(CO)$_4$(η^2-*(Z)*-cyclooctene)$_2$: $C_{20}H_{28}O_4W$, colorless crystals, molecular weight 516.3 g·mol^{-1}, crystal size 0.15 × 0.36 × 0.37 mm, a = 7.504(1) Å, b = 12.652(2) Å, c = 21.445(5) Å, β = 95.48(1)°, V = 2026.7(5) Å^3, T = 293 K, d_{calc} = 1.69 g·cm^{-3}, μ = 58.4 cm^{-1}, Z = 4, monoclinic, space group $P2_1/c$ (no.14), Enraf-Nonius-CAD4 diffractometer, $\omega-2\theta$ scan mode, λ = 0.71069 Å, empirical absorption correction (min. 0.931, max. 1.000), 4567 measured reflections ($\pm h,+k,+l$), $[(\sin\theta)/\lambda]_{max}$ 0.66 Å^{-1}, 4567 independent and 3242 observed reflections [$I \geq 2\sigma(I)$], 226 refined parameter, heavy atom method, H atom positions were calculated, R_1 = 0.028, R_w = 0.035 [$w = 1/\sigma^2(F_o)$], residual electron density 0.72 e Å^{-3}. The molecular structure in the crystal essentially shows a square-planar arrangement of the four carbonyl ligands around the metal center [W−C distances: 2.041(5), 2.044(5), 2.031(6), and 2.066(6) Å] and trans-orthogonal orientation of the C=C double bonds of the two olefin ligands [W−C distances: 2.351(6), 2.355(6), 2.360(5), and 2.360(6) Å] which are eclipsed to the respective OC−W−CO axes.

(41) Heinemann, F.; Schmidt, H.; Peters, K.; Thiery, D. *Z. Kristallogr.* **1992**, *198*, 123−124. The structure of W(CO)$_6$ (**1**) in the crystal is essentially octahedral, although it shows slightly varying W−C (2.018−2.032 Å) and C−O (1.130−1.158 Å) distances, as calculated from the published atomic coordinates.

Scheme 2

$W(CO)_5(\eta^2\text{-}Me_3Si\text{-}C{\equiv}C\text{-}SiMe_3)$ + 2 eco

20 °C ↓

cis-$W(CO)_4(\eta^2\text{-eco})_2$ + $Me_3Si\text{-}C{\equiv}C\text{-}SiMe_3$ + CO

3

Scheme 3

$W(CO)_4(\eta^4\text{-1,4-diphenylbutadiene})$ + 2 eco

20 °C ↓

cis-$W(CO)_4(\eta^2\text{-eco})_2$ + 1,4-diphenylbutadiene

3

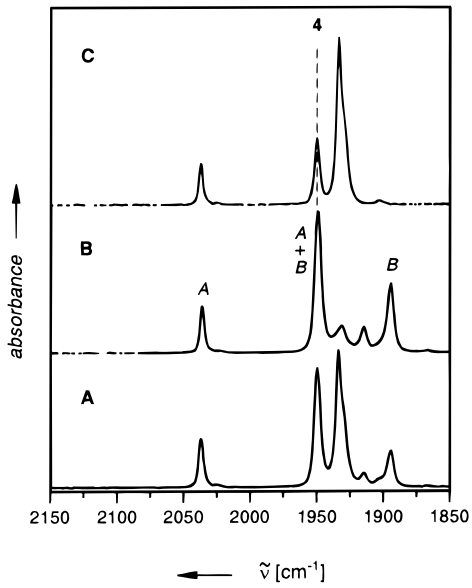

Figure 2. IR spectra of *cis*-$W(CO)_4(\eta^2\text{-eco})_2$ (**3**) in the ν(CO) region, recorded in *n*-hexane: (A) spectrum of a mixture of **3a** (meso form) and **3b** (racemate); (B) spectrum of *cis*-$W(CO)_4[\eta^2\text{-}(-)\text{eco}]_2$ (enantiomer **3b″**) [2035.8 (*A*), 1948.6 (*A* and *B*, overlapping), 1930.7, 1914.2, and 1894.1 (*B*) cm^{-1}] generated using pure (−)-*(E)*-cyclooctene; (C) spectrum of **3a** [2037.3, 1950.0, 1933.4, and 1929 (sh) cm^{-1}] obtained from the spectrum of the **3a**+**3b** mixture by computer-assisted removal of the whole spectrum of **3b″**. The vertical dashed line indicates where the strong absorption of *trans*-$W(CO)_4(\eta^2\text{-eco})_2$ (**4**) would appear (1949.9 cm^{-1}).

***cis*-Tetracarbonylbis(η^2-*(E)*-cyclooctene)tungsten (3).** Complex **3** is difficult to isolate from the reaction mixtures photochemically generated according to Scheme 1. However, analytically pure samples are accessible via independent thermal routes involving either the reaction of a $W(CO)_5(\eta^2\text{-alkyne})$ complex[29] with *(E)*-cyclooctene (Scheme 2) or the displacement of the diene in a $W(CO)_4(\eta^4\text{-diene})$ complex[31] by *(E)*-cyclooctene (Scheme 3).

The IR spectra of various samples of **3** exhibit up to six discernible absorptions in the CO stretching vibrational region. An illustrative spectrum, with frequencies extending over a range of about 140 cm^{-1}, is displayed in Figure 2A. It resembles the type of ν(CO) pattern previously reported for several in situ photogenerated *cis*-$W(CO)_4(\eta^2\text{-alkene})_2$ complexes.[3,5,15,16,18,19] However, the number of bands and the variations, from sample to sample, in the relative intensities indicate that the spectra represent mixtures of two species.

By analogy with the *trans*-$W(CO)_4(\eta^2\text{-eco})_2$ complexes **4a** and **4b**, two different products can also be expected for *cis*-$W(CO)_4(\eta^2\text{-eco})_2$ (**3**), viz., a meso-compound (**3a**) of composition *cis*-$W(CO)_4[\eta^2\text{-}(+)\text{-eco}][\eta^2\text{-}(-)\text{-eco}]$ and a racemate (**3b**) of the two enantiomers *cis*-$W(CO)_4[\eta^2\text{-}(+)\text{-eco}]_2$ (**3b′**) and *cis*-$W(CO)_4[\eta^2\text{-}(-)\text{-eco}]_2$ (**3b″**).

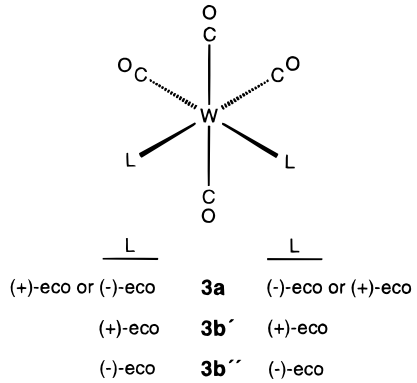

In accordance with this notion, the ^{13}C NMR spectra of various samples of **3** showed indeed two sets of signals. The two isomers are clearly distinguishable on the basis of the number of carbonyl resonances: **3a**, with (virtual) C_s symmetry, exhibits three lines with 2:1:1 relative intensities, while two lines with equal intensities are observed for **3b** with (virtual) C_2 symmetry.

Two sets of four lines each are observed for the *(E)*-cyclooctene ligands in the $^{13}C\{^1H\}$ NMR spectrum of the **3a**+**3b** mixture, thus confirming the position of the olefins in chemically equivalent environments and, moreover, indicating that the rotation about the metal−olefin bond axes in either of the two compounds is rapid on the NMR time scale. The olefinic carbon atoms exhibit a coordination shift[42] to higher field, $\Delta\delta = 52.3$ for **3a** and 47.2 for **3b**. This is much smaller than that observed for the *trans*-$W(CO)_4(\eta^2\text{-eco})_2$ complexes **4a** and **4b** ($\Delta\delta = 76.2$ and 75.9, respectively). The difference of ca. 25 ppm is similar to the values previously reported for various other olefins in related pairs of compounds[43] in which an olefin ligand is either trans-orthogonal to a second olefin ligand or trans to a CO group. These observations not only confirm the structural assignment of *cis*-$W(CO)_4(\eta^2\text{-eco})_2$ (**3a** and **3b)** but also further substantiate the relevance of coordination shift data as a general criterion in recognizing the position of an olefinic unit relative to other ligands in octahedral complexes.[43]

Despite the exceptional coordination ability of *(E)*-cyclooctene, *cis*-$W(CO)_4(\eta^2\text{-eco})_2$ (**3**) decomposes slowly in solution at ambient temperature, unless an excess of free *(E)*-cyclooctene is present. The solid material can nevertheless be handled at ambient temperature, although cooling is recommended for long-term storage.

To find a sound basis for monitoring the concentration of *cis*-$W(CO)_4\text{-}(\eta^2\text{-eco})_2$ (**3**) as an intermediate in the photochemical formation of *trans*-$W(CO)_4(\eta^2\text{-eco})_2$ (**4**) (Scheme 1) by means of quantitative IR spectroscopy,

(42) ^{13}C NMR chemical shifts of free *(E)*-cyclooctene: $\delta = 133.91$, 36.03, 35.88, and 29.46 (in toluene-d_8).

(43) Grevels, F.-W.; Jacke, J.; Betz, P.; Krüger, C.; Tsay, Y.-H. *Organometallics* **1989**, *8*, 293−298.

efforts were made to disentangle the overlapping ν(CO) bands in the changeable IR spectra of **3** (Figure 2A) and to identify the individual patterns associated with the two isomers, **3a** and **3b**. However, none of the attempts to separate these compounds by fractional crystallization scored a lasting success, such that no reliable quantitative IR spectra could be recorded. This is due to the interconversion of **3a** and **3b**, albeit slow, in solution at ambient temperature which, logically, involves the exchange of coordinated (+)- and (−)-*(E)*-cyclooctene with the respective other enantiomer of the free olefin added to the solution for the purpose of preventing the complex from decomposition (Scheme 4).

Scheme 4

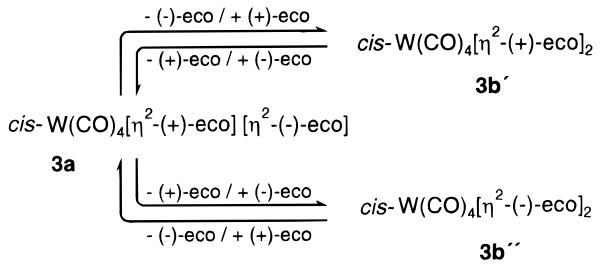

The obvious strategy to circumvent this problem is to preclude the formation of the meso-compound **3a** by using only one enantiomer of *(E)*-cyclooctene in the synthesis according to Scheme 3. Thus, W(CO)$_4$(η^4-*(E,E)*-1,4-diphenyl-1,3-butadiene)[31] was quantitatively converted into *cis*-W(CO)$_4$[η^2-(−)-eco]$_2$ (**3b″**) by the reaction with a 10-fold excess of (−)-*(E)*-cyclooctene (≥99.5% enantiomeric purity). The resulting IR spectrum exhibits three prominent absorptions in the CO stretching vibrational region (Figure 2B), in close similarity with the ν(CO) pattern [A_1, A_1 and B_1 (overlapping), and B_2] of the related compounds M(CO)$_4$($\eta^{2:2}$-diene) (M = Mo, W; diene = 1,5-cyclooctadiene,[44] norbornadiene[45]), where the two C=C units naturally are in mutual cis position and oriented parallel to each other. This latter structural feature is reasonably adapted to **3b**, along with the assignment of the ν(CO) modes [A, A and B (overlapping), and B].

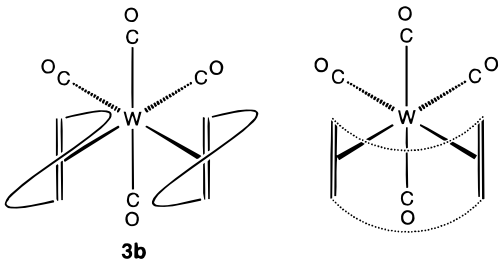

The ν(CO) pattern of the meso-compound **3a** (Figure 2C) is readily obtained from the spectrum of **3a**+**3b** (Figure 2A) by computer-assisted removal of the spectrum associated with **3b**. Again consistent with the proposed *cis*-M(CO)$_4$L$_2$ structure, it shows three well-resolved bands and a shoulder at the low-frequency side of the strongest absorption. However, the distinctly different shape of the spectrum, compared with **3b**, indicates a different influence of the olefin ligands on the carbonyl groups. It seems plausible to attribute this to a different mutual orientation of the C=C units, enforced by some steric constraints arising from the face-to-face arrangement of the two enantiomers of *(E)*-cyclooctene. Similar considerations seem applicable to postulate a conformer of **3b** which may be present in low equilibrium concentration and, thus, would give rise to the unassigned minor absorptions in Figure 2B.

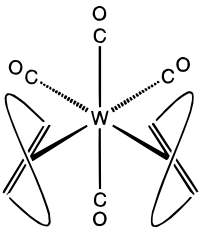

3a

Once the individual ν(CO) spectra of **3a** and **3b** were available, solutions of **3** could be analyzed on a quantitative level. In this way it was found that the reaction in Scheme 3 initially generates the two isomers in equimolar amounts. Upon standing at ambient temperature, the ratio gradually changes in favor of **3a** and approaches, after several hours, an equilibrium value of 3:1.

It has been suggested[5] that *cis*- and *trans*-M(CO)$_4$(η^2-alkene)$_2$ complexes coexist in a thermal equilibrium which favors the thermodynamically more stable trans isomers. Our observations made with *(E)*-cyclooctene as the olefin ligand do not support this suggestion, although it cannot entirely be ruled out for other, less strongly bound olefins. As a matter of fact, all purified samples of *cis*- and *trans*-W(CO)$_4$(η^2-eco)$_2$ (**3** and **4**) were free of the respective other isomer, as proven by NMR spectroscopy. Particularly worth emphasizing, the IR ν(CO) pattern of *cis*-W(CO)$_4$[η^2-(−)-eco]$_2$ (Figure 2B) remained virtually unchanged with time. An increase in the absorption band at 1950 cm^{-1} at the expense of the other spectral features, which would have been indicative of the formation of *trans*-W(CO)$_4$[η^2-(−)-eco]$_2$, was not observed, even after many hours at ambient temperature.

The isomerization of *cis*- to *trans*-W(CO)$_4$(η^2-eco)$_2$ (**3** → **4**) is exclusively a photochemical process. Quantum yield measurements were performed, in the presence of a 10-fold excess of *(E)*-cyclooctene, by irradiating at λ = 365 nm into the long-wavelength tail end of the electronic absorption spectrum of **3** (Figure 3). At this wavelength, the electronic absorption of **4** (Figure 3) is low (ϵ = 170 L·mol^{-1}·cm^{-1}) in comparison with that of **3** (ϵ = 1540 L·mol^{-1}·cm^{-1}) so that internal light filtering can be ignored in the evaluation of the quantum yield as long as the conversion is not too high. At up to 40−50% conversion, plots of the concentrations of **3** and **4** versus the total amount of absorbed light give indeed virtually straight lines (Figure 4), the slopes of which represent the respective quantum yields.

It has to be noted that the irradiation of **3** not only gives rise to the cis → trans isomerization with formation of **4** but also disturbs the equilibrium of the two isomers of the cis complex, **3a** ⇌ **3b**. In other words, complex **3** is not represented by a uniform ν(CO) intensity pattern which could directly be used to determine its concentration in the reaction mixtures by

(44) Kayran, C.; Kozanoglu, F.; Özkar, S.; Saldamli, S.; Tekkaya, A.; Kreiter, C. G. *Inorg. Chim. Acta* **1999**, *284*, 229−236.

(45) Darensbourg, D. J.; Nelson, H. H., III; Murphy, M. A. *J. Am. Chem. Soc.* **1977**, *99*, 896−903.

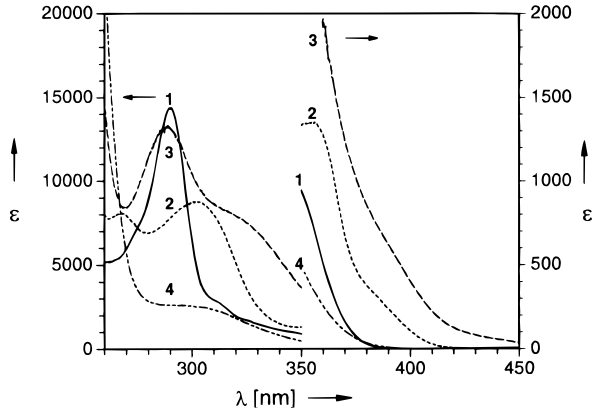

Figure 3. UV−vis absorption spectra of $W(CO)_6$ (**1**), $W(CO)_5(\eta^2\text{-eco})$ (**2**), *cis*-$W(CO)_4(\eta^2\text{-eco})_2$ (**3**), and *trans*-$W(CO)_4(\eta^2\text{-eco})_2$ (**4**), recorded in *n*-hexane.

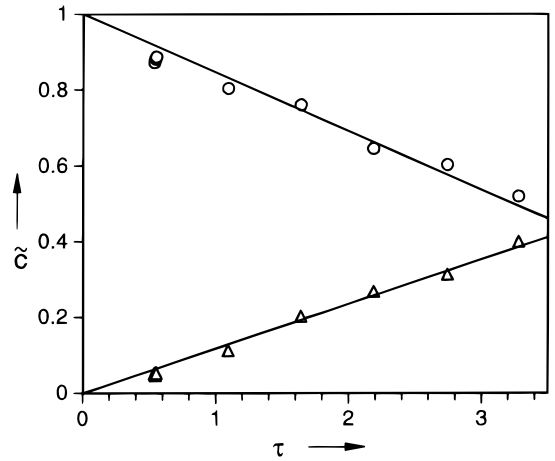

Figure 4. Photochemical conversion of *cis*-$W(CO)_4(\eta^2\text{-eco})_2$ (**3**, ○) into *trans*-$W(CO)_4(\eta^2\text{-eco})_2$ (**4**, △) upon irradiation (λ = 365 nm) in *n*-hexane solution containing *(E)*-cyclooctene. The slope of $\tilde{c}_3 = f(\tau)$ yields $\Phi_{34} = 0.15$. The concentrations ($\tilde{c}_i$) and the absorbed amount of light (τ) are normalized to the initial concentration of the starting material (**3**).[34]

means of quantitative IR spectroscopy. Rather, the concentration of **3** has to be evaluated as the sum of the individual concentrations of the two isomers. In detail, the analysis involves the determination of c_{3b} and the computer-assisted removal of the entire ν(CO) spectrum of **3b** (cf. Figure 2B) on the basis of the absorbance at 1894.1 cm^{-1}, followed by the determination of c_{3a} and the computer-assisted removal of the entire ν(CO) spectrum of **3a** (cf. Figure 2C) on the basis of the absorbances at 2037.3 and 1933.4 cm^{-1}, leaving behind the strong absorption of **4** at 1949.9 cm^{-1} as a basis for the determination of c_4. The latter absorption nearly coincides with one band each of **3a** (1950.0 cm^{-1}) and **3b** (1948.6 cm^{-1}), so that the procedure is prone to experimental errors, and a high level of accuracy is required in order to achieve reliable results. Moreover, the system is very sensitive to traces of oxygen, which, particularly under photolytic conditions, gives rise to oxidative decomposition with loss of material. Therefore, rigorous degassing is indispensable in order to achieve a satisfactory material balance.

In view of all these possible sources of error it is not surprising that the quantum yields for the disappearance of **3** and the formation of **4** were somewhat found to scatter: $\Phi_{-3} = 0.15$ and $\Phi_{+4} = 0.12$. Because of the slightly deficitary material balance (92−94%), we take

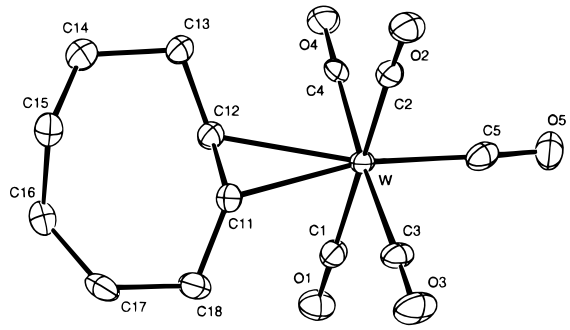

Figure 5. Structure of $W(CO)_5(\eta^2\text{-eco})$ (**2**) in the crystal.

the higher value as the cis → trans isomerization quantum yield, $\Phi_{34} = 0.15$.

The reverse process, the trans → cis photoisomerization of $W(CO)_4(\eta^2\text{-olefin})_2$, has recently been observed in low-temperature media,[16,17] but is negligible under the conditions of our experiments. This is evident from control experiments involving the irradiation of **4** in the presence of excess *(E)*-cyclooctene at λ = 365, which indicate an upper limit for the quantum yield Φ_{43} on the order of 0.01.

Pentacarbonyl(η^2-*(E)*-cyclooctene)tungsten (2). Thermal ligand exchange using $W(CO)_5(\eta^2\text{-zco})$[7,28] as a source of the $W(CO)_5$ unit is a convenient route to complex **2** (Scheme 5), providing nearly quantitative yield.

Scheme 5

$$W(CO)_5(\eta^2\text{-zco}) + \text{eco} \xrightarrow{\Delta} W(CO)_5(\eta^2\text{-eco}) + \text{zco}$$

2

The X-ray structure analysis of **2** in essence shows an octahedral coordination geometry (Figure 5, Table 2). The C═C bond of the *(E)*-cyclooctene ligand is eclipsed to one of the two equatorial OC−W−CO axes of the square-pyramidal $W(CO)_5$ skeleton, as indicated by the respective C(carbonyl)−W−C(11)−C(12) torsional angles. This is in accord with the results of a theoretical study of $W(CO)_5(\eta^2\text{-ethene})$,[46] where the eclipsed orientation of the C═C double bond was predicted to be slightly favored over the staggered structure. A nearly eclipsed structure was previously found for $W(CO)_5(\eta^2\text{-zco})$.[7,47] Comparison of the W−C(olefin) bond lengths in the latter compound (2.49 and 2.51 Å)[7] with those in **2** [W−C(11) = 2.451(5) Å, W−C(12) = 2.425(4) Å; Table 2] again underlines that *(E)*-cyclooctene is indeed significantly stronger bound than *(Z)*-cyclooctene.

It is interesting to compare the W−C bond distances to the olefinic ligands and the C═C bond lengths in **2** and **4a** (Table 2). The W−C bond distances to the olefinic carbons in **2** [W−C(11) = 2.451(5) and W−C(12) = 2.425(4) Å] are distinctly longer than those in **4a** [W−C(12) = W−C(12*) = 2.327(3), W−C(22) = W−C(22*) = 2.328(3) Å], while the C═C bond lengths show the opposite trend [**2,** C(11)−C(12) = 1.384(6) Å; **4a**, C(12)−

(46) (a) Pidun, U.; Frenking, G. *Organometallics* **1995**, *14*, 5325−5336. (b) Pidun, U. Diploma Thesis; Universität Marburg, 1995.

(47) In the discussion concerning the structure of $W(CO)_5(\eta^2\text{-}(Z)\text{-cyclooctene})$,[7] the C═C double bond was mentioned to be staggered with the carbonyl ligands. However, the calculation of the four C(olefin)−C(olefin)−W−C(equatorial carbonyl) torsional angles (170.9°, 81.8°, −8.0°, and −97.3°) from the published atomic coordinates reveals that the C═C bond actually is not far from being eclipsed to one of the two OC−W−CO axes and perpendicular to the other.

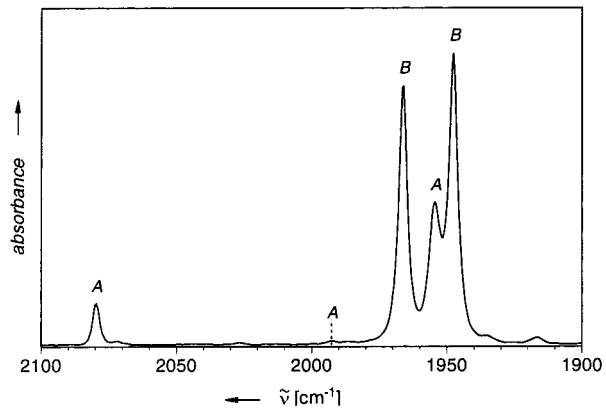

Figure 6. IR spectrum of $W(CO)_5(\eta^2$-eco) (**2**) in the ν(CO) region [2079.5 (*A*), 1992.2 (*A*), 1966.1 (*B*), 1954.3 (*A*), 1947.4 (*B*) cm^{-1}], recorded in *n*-hexane.

C(12*) = 1.424(5) Å and C(22)−C(22*) = 1.412(6) Å]. This indicates a considerable strengthening of the metal−olefin bond on passing from **2** to **4a**, in accord with the notion of an enhanced metal d(π) → olefin(π*) back-donation arising from the single-faced nature of the olefinic ligands and their trans-orthogonal arrangement in **4a**. In complex **2**, the CO group trans to the olefin effectively competes with the olefin for π back-donation and thus renders the metal−olefin bond weaker than in **4a**.

The $W(CO)_5$ skeleton of **2** in the crystal is somewhat distorted from the C_2 molecular symmetry of the complex. The four equatorial CO ligands are not pairwise equivalent, but differ by ca. 0.02 Å in each pair [W−C(1)/C(2) = 2.047(5)/2.069(5), W−C(3)/C(4) = 2.050(5)/2.031(4) Å]. Similar distortions were found for the parent $W(CO)_6$ (**1**) in the crystal,[39,41] thus illustrating that crystal packing effects may be difficult to separate from subtle, but chemically relevant variations in the M−CO bonding situation.

The IR spectrum of **2** exhibits four prominent bands in the CO stretching vibrational region (Figure 6) instead of the typical three-band pattern commonly observed for $M(CO)_5L$ complexes with (local) C_{4v} symmetry [3 IR active ν(CO) modes: 2 A_1, E].[48] Obviously, the degeneracy of the E mode is lifted, due to the single-face π-acceptor character of the olefin ligand. At C_2 symmetry, all five ν(CO) modes [3 A, 2 B] are IR active. However, one has to keep in mind that one of the three A modes corresponds to the IR inactive B_2 mode of the undistorted fragment and, therefore, is intrinsically weak in intensity. The two strongest bands in the spectrum apparently correspond to the two components of the very intense E mode at C_{4v} symmetry and thus are assigned as the B modes of **2**. The knowledge of the CO force constants would be very helpful with respect to a better understanding of the directional influence of the olefin ligand on the individual CO groups of the $W(CO)_5$ moiety. However, the evaluation of such data requires complementary frequencies of ^{13}CO-labeled derivatives,[49] since a rigorous treatment of the $W(CO)_5$ unit with C_2 symmetry within the framework of the energy-factored CO force field approximation,[50−52] involves a total number of nine parameters (three principal and six interaction force constants).

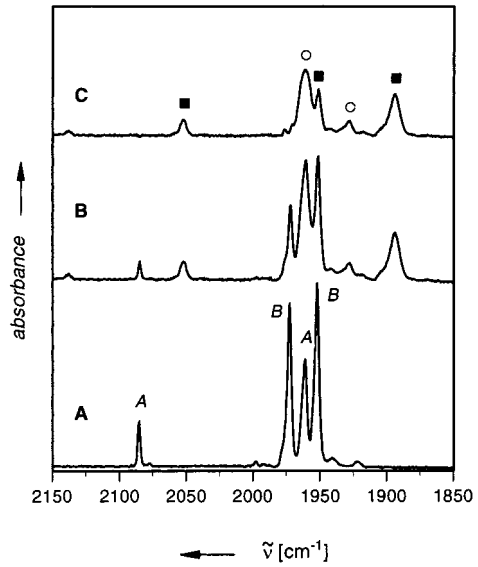

Figure 7. IR Spectra in the ν(CO) region from a low-temperature matrix experiment with $W(CO)_5(\eta^2$-eco) (**2**) in solid argon at 10 K: (A) after deposition [2084.9, 1972.2, 1961.0, 1951.8 cm^{-1}]; (B) after 30 min irradiation (λ = 334 nm); (C) difference spectrum [spectrum B − (0.32 × spectrum A)], indicating the formation of the fragments $W(CO)_5$ [○; 1961.5 and 1928 cm^{-1}] and $W(CO)_4(\eta^2$-eco) [■; 2052.5, 1951.5, and 1894 cm^{-1}].

The ^{13}C NMR spectrum of **2** shows, in addition to the resonances associated with the *(E)*-cyclooctene ligand, two lines in the carbonyl region in an approximately 4:1 ratio. The appearance of only one signal for the four equatorial CO groups, even at temperatures down to 193 K, indicates that the molecule is highly fluxional with respect to rotation about the metal−olefin bond axis. The coordination shift to higher field of the olefin carbon atoms,[42] $\Delta\delta$ = 50.0, is in accord with the value expected for *(E)*-cyclooctene in trans position to a CO group (cf. the corresponding data of **3**).

The photochemistry of $W(CO)_5(\eta^2$-eco) (**2**) involves two primary processes, loss of CO and detachment of the olefin ligand, as monitored by IR spectroscopy under low-temperature matrix isolation conditions (Scheme 6).

Scheme 6

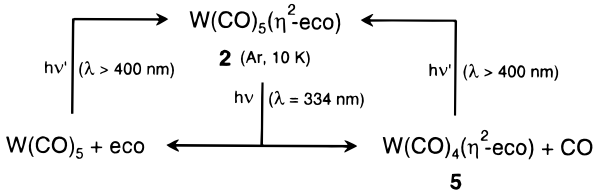

The CO stretching vibrational pattern of **2**, deposited in argon at 10 K, is displayed in Figure 7A. Upon irradiation at λ = 334 nm (Figure 7B), the high-frequency A band (2084.9 cm^{-1}) and the two B bands (1972.2 and 1951.8 cm^{-1}) of **2** gradually decrease, while three new bands grow in at 2052.5, 1928, and 1894,

(48) Braterman, P. S. *Metal Carbonyl Spectra*; Academic Press: London, 1975.

(49) A comparative investigation into the energy-factored CO force field of $W(CO)_6$ (**1**), $W(CO)_5(\eta^2$-eco) (**2**), and *trans*-$W(CO)_4(\eta^2$-eco)$_2$ (**4**), including the syntheses of ^{13}CO-labeled derivatives, is in progress and will be communicated elsewhere.

(50) Cotton, F. A.; Kraihanzel, C. S. *J. Am. Chem. Soc.* **1962**, *84*, 4432−4438.

(51) Haas, H.; Sheline, R. K. *J. Chem. Phys.* **1967**, *47*, 2996−3021.

(52) Bor, G. *Inorg. Chim. Acta* **1967**, *1*, 81−92.

along with a weak feature at 2138 cm^{-1}, which is readily assigned to free CO. The absorption at the position of the low-frequency A vibration (1961 cm^{-1}) of **2** maintains nearly its initial intensity, which indicates that an additional product absorption band emerges at almost the same frequency. This becomes more obvious when the residual absorptions of the starting material **2** are removed by computer-assisted subtraction (Figure 7C). Comparison with literature data[53] identifies the bands at 1928 and 1961.5 cm^{-1} as the low-frequency A_1 and E modes of the $W(CO)_5$ fragment, respectively. The other three product bands at 2052.5, 1951.5, and 1894 cm^{-1} are logically attributed to the CO loss product, the $W(CO)_4(\eta^2$-eco) fragment (**5**). Subsequent long-wavelength irradiation ($\lambda \geq 400$ nm), i.e., into a broad band emerging in the electronic spectrum at around 420 nm, resulted in partial reformation of **2** at the expense of both of the two fragments, thus indicating that both of them absorb in this spectral region and undergo photoinduced re-coordination of the respective photodissociated ligand from the matrix cage environment.

The observed ν(CO) pattern of **5** is consistent with a "seesaw"-type arrangement of the carbonyl ligands in the $W(CO)_4$ unit[48] rather than a square-planar $W(CO)_4$ skeleton. In the latter case, only one strong ν(CO) absorption (or a closely spaced pair of bands) would be expected, as long as the $W(CO)_4$ moiety is not too much distorted from planarity.

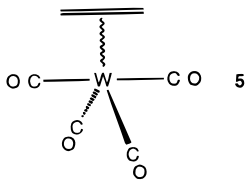

5

Photokinetics and Quantum Yields. The overall process of the formation of *trans*-$W(CO)_4(\eta^2$-eco$)_2$ (**4**) from $W(CO)_6$ (**1**) and excess *(E)*-cyclooctene essentially involves three consecutive photochemical steps (Scheme 7).

Scheme 7

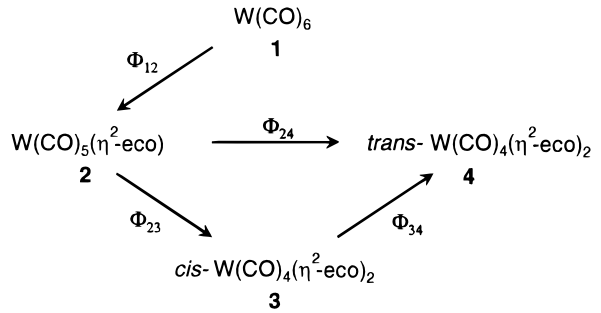

In contrast to the gas-phase photolysis of $W(CO)_6$ (**1**) in the presence of ethene with formation of $W(CO)_4(\eta^2$-ethene$)_2$,[19] there is no indication of any direct conversion of **1** into either of the two disubstituted products **3** and **4** in our solution experiments. However, the direct photoproduction of **4** from **2** cannot a priori be excluded and, therefore, is accounted for in Scheme 7. Any reverse process involving replacement of *(E)*-cyclooctene by CO can be left out of consideration under the conditions employed, i.e., in the presence of a large excess of the olefin under inert atmosphere.

As shown in the Appendix, the concentrations of the starting material and the products in such a sequence of photoreactions can be obtained as implicit functions of the total amount of light absorbed by the system, the quantum yields of the individual photoprocesses, and the UV−vis molar absorbance coefficients of the compounds involved. The functional relationships derived in the Appendix (eqs A-12, A-8, A-10, and A-11) refer to a four-component system (A, B, C, and D) involving six photoprocesses with the quantum yields Φ_{AB}, Φ_{AC}, Φ_{AD}, Φ_{BC}, Φ_{BD}, and Φ_{CD}, but are readily adapted to the special case given in Scheme 7 by setting $\Phi_{AB} = \Phi_{12}$, $\Phi_{AC} = \Phi_{AD} = 0$, $\Phi_{BC} = \Phi_{23}$, $\Phi_{BD} = \Phi_{24}$, and $\Phi_{CD} = \Phi_{34}$. Furthermore, for convenience the concentrations (c_i) of the four compounds and the total amount of light absorbed by the system are normalized to the initial concentration (c_1^0) of the starting material by setting $c_i/c_1^0 = \tilde{c}_i$ and $(1/c_1^0)\int_0^t Q_{abs}\,dt = \tau$. With these substitutions one obtains the functional relationships of eqs 1−4.

$$p_1[1-\tilde{c}_1] + p_2[1-\tilde{c}_1^{\beta}] + p_3[1-\tilde{c}_1^{\gamma}] - \epsilon_4 \ln \tilde{c}_1 = \epsilon_1\Phi_{12}\tau \quad (1)$$

$$\frac{\tilde{c}_2}{\tilde{c}_1} = q[\tilde{c}_1^{(\beta-1)} - 1] \quad (2)$$

$$\frac{\tilde{c}_3}{\tilde{c}_1} = r_1 + r_2\tilde{c}_1^{(\beta-1)} + r_3\tilde{c}_1^{(\gamma-1)} \quad (3)$$

$$\tilde{c}_4 = 1 - \tilde{c}_1 - \tilde{c}_2 - \tilde{c}_3 \quad (4)$$

where $\beta = \dfrac{\epsilon_2(\Phi_{23}+\Phi_{24})}{\epsilon_1\Phi_{12}}$ $\qquad$ $\gamma = \dfrac{\epsilon_3\Phi_{34}}{\epsilon_1\Phi_{12}}$

$$p_1 = (\epsilon_1 - \epsilon_4) - \frac{(\epsilon_2-\epsilon_4)}{(1-\beta)} + \frac{(\epsilon_3-\epsilon_4)}{(1-\gamma)}\frac{\beta}{(1-\beta)}\frac{\Phi_{23}}{(\Phi_{23}+\Phi_{24})}$$

$$p_2 = \frac{(\epsilon_2-\epsilon_4)}{\beta(1-\beta)} + \frac{(\epsilon_3-\epsilon_4)}{(1-\beta)(\gamma-\beta)}\frac{\Phi_{23}}{(\Phi_{23}+\Phi_{24})}$$

$$p_3 = \frac{(\epsilon_3-\epsilon_4)}{\gamma(1-\gamma)}\frac{\beta}{(\beta-\gamma)}\frac{\Phi_{23}}{(\Phi_{23}+\Phi_{24})}$$

$$q = \frac{1}{(1-\beta)}$$

$$r_1 = \frac{1}{(1-\gamma)}\frac{\beta}{(1-\beta)}\frac{\Phi_{23}}{(\Phi_{23}+\Phi_{24})}$$

$$r_2 = \frac{\beta}{(1-\beta)(\gamma-\beta)}\frac{\Phi_{23}}{(\Phi_{23}+\Phi_{24})}$$

$$r_3 = \frac{1}{(1-\gamma)}\frac{\beta}{(\beta-\gamma)}\frac{\Phi_{23}}{(\Phi_{23}+\Phi_{24})}$$

These equations can be numerically solved for the concentrations. Using a given set of quantum yields and

(53) (a) Graham, M. A.; Poliakoff, M.; Turner, J. J. *J. Chem. Soc. (A)* **1971**, 2939−2948. (b) Perutz, R. N.; Turner, J. J. *Inorg. Chem.* **1975**, *14*, 262−270. (c) Perutz, R. N.; Turner, J. J. *J. Am. Chem. Soc.* **1975**, *97*, 4791−4800.

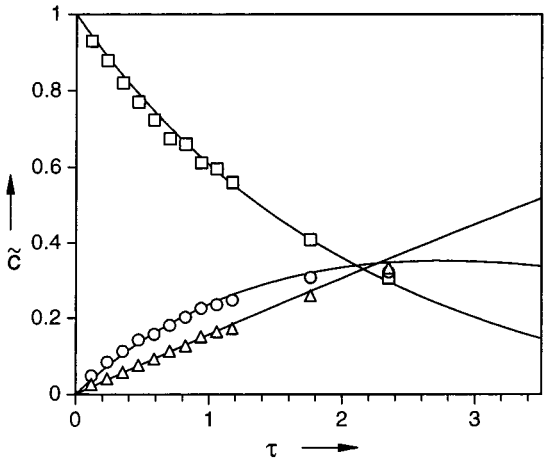

Figure 8. Photochemical conversion of $W(CO)_5(\eta^2\text{-eco})$ (**2**, □) into *cis*-$W(CO)_4(\eta^2\text{-eco})_2$ (**3**, ○) and *trans*-$W(CO)_4(\eta^2\text{-eco})_2$ (**4**, △) upon irradiation (λ = 365 nm) in the presence of excess *(E)*-cyclooctene in *n*-hexane solution. The symbols indicate the experimental data points, while the curves represent $\tilde{c}_i = f(\tau)$ computed with $\Phi_{23} = 0.34$, $\Phi_{24} = 0.16$, $\Phi_{34} = 0.15$, and the ϵ values of the involved complexes. The concentrations ($\tilde{c}_i$) and the absorbed amount of light (τ) are normalized to the initial concentration of the starting material (**2**).[34]

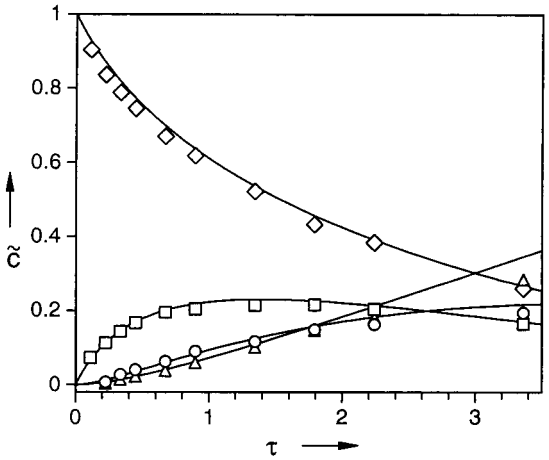

Figure 9. Photochemical conversion of $W(CO)_6$ (**1**, ◇) into $W(CO)_5(\eta^2\text{-eco})$ (**2**, □), *cis*-$W(CO)_4(\eta^2\text{-eco})_2$ (**3**, ○), and *trans*-$W(CO)_4(\eta^2\text{-eco})_2$ (**4**, △) upon irradiation (λ = 365 nm) in the presence of excess *(E)*-cyclooctene in *n*-hexane solution. The symbols indicate the experimental data points, while the curves represent $\tilde{c}_i = f(\tau)$ computed with $\Phi_{12} = 0.73$, $\Phi_{23} = 0.34$, $\Phi_{24} = 0.16$, $\Phi_{34} = 0.15$, and the ϵ values of the involved complexes. The concentrations ($\tilde{c}_i$) and the absorbed amount of light (τ) are normalized to the initial concentration of the starting material (**1**).[34]

molar absorbance coefficients, the concentrations can thus be computed as functions of the absorbed amount of light. With these functional relationships the quantum yields can be evaluated in an iterative way on the basis of a sufficiently large number of experimental data as follows.

In two series of experiments $W(CO)_6$ (**1**) and $W(CO)_5(\eta^2\text{-eco})$ (**2**), respectively, were irradiated in the presence of a 10-fold excess of *(E)*-cyclooctene for varying periods of time. In each individual run the total amount of light absorbed by the system was measured with an electronically integrating actinometer, while the concentrations of the starting materials and products were determined by quantitative IR spectroscopy. UV−vis spectroscopy is clearly not suitable for this purpose because of the broadness and the substantial overlap of the absorption bands throughout the entire spectral region (Figure 3).

In principle, the quantum yields of all four processes involved in the overall reaction (Scheme 7) can be determined from the experiments starting with $W(CO)_6$ (**1**). However, for the sake of accuracy the quantum yields Φ_{23} and Φ_{24} were separately determined from the irradiation of $W(CO)_5(\eta^2\text{-eco})$ (**2**) in the presence of a 10-fold excess of *(E)*-cyclooctene, taking $\Phi_{34} = 0.15$ as a fixed value known already from the cis → trans photoisomerization of $W(CO)_4(\eta^2\text{-eco})_2$ (**3** → **4**, vide supra).

The gradual conversion of **2** into **3** and **4** upon irradiation with $\lambda = 365$ nm is displayed in Figure 8. It includes the results of 12 individual runs with a conversion of the starting material up to 70% and a satisfactory material balance throughout (≥96%). The concentration of the intermediate product **3** reaches a maximum of ca. 33% of the entire reaction mixture. The quantum yields Φ_{23} and Φ_{24} were evaluated on the basis of eqs 5−7, which are adapted from the Appendix (eqs A13−A15) by setting $\Phi_{AB} = \Phi_{23}$, $\Phi_{AC} = \Phi_{24}$, $\Phi_{BC} = \Phi_{34}$ (=0.15) and normalizing the concentrations and the absorbed amount of light to the initial concentration of the starting material **2** ($c_i/c_2^0 = \tilde{c}_i$, and $(1/c_2^0)\int_0^t Q_{abs}\, dt = \tau$).

$$u_1[1 - \tilde{c}_2] + u_2[1 - \tilde{c}_2^{\beta}] - \epsilon_4 \ln \tilde{c}_2 = \epsilon_2(\Phi_{23} + \Phi_{24})\tau \tag{5}$$

$$\frac{\tilde{c}_3}{\tilde{c}_2} = q[\tilde{c}_2^{(\beta - 1)} - 1] \tag{6}$$

$$\tilde{c}_4 = 1 - \tilde{c}_2 - \tilde{c}_3 \tag{7}$$

where $\beta = \dfrac{\epsilon_3\Phi_{34}}{\epsilon_2(\Phi_{23} + \Phi_{24})}$

$$u_1 = (\epsilon_2 - \epsilon_4) - \frac{(\epsilon_3 - \epsilon_4)}{(1 - \beta)} \frac{\Phi_{23}}{(\Phi_{23} + \Phi_{24})}$$

$$u_2 = \frac{(\epsilon_3 - \epsilon_4)}{\beta(1 - \beta)} \frac{\Phi_{23}}{(\Phi_{23} + \Phi_{24})}$$

$$q = \frac{1}{(1 - \beta)} \frac{\Phi_{23}}{(\Phi_{23} + \Phi_{24})}$$

Starting with a reasonable guess for the quantum yields Φ_{23} and Φ_{24}, the concentrations ($\tilde{c}_2$, $\tilde{c}_3$, $\tilde{c}_4$) were computed as functions of the amount of absorbed light (τ). In an iterative procedure[54] the quantum yield input data were varied until the best fit of the computed concentrations to the measured concentrations was achieved (Figure 8): $\Phi_{23} = 0.34$ and $\Phi_{24} = 0.16$.

These quantum yields were used as fixed input values in the analogous treatment of the experimental data obtained from the irradiation of $W(CO)_6$ (**1**) under the same conditions (λ = 365 nm, 10-fold excess of *(E)*-cyclooctene), yielding $\Phi_{12} = 0.73$. The combined results of 10 individual runs are displayed in Figure 9. Again,

(54) The Fortran computer program is available on request from one of the authors (F.M.).

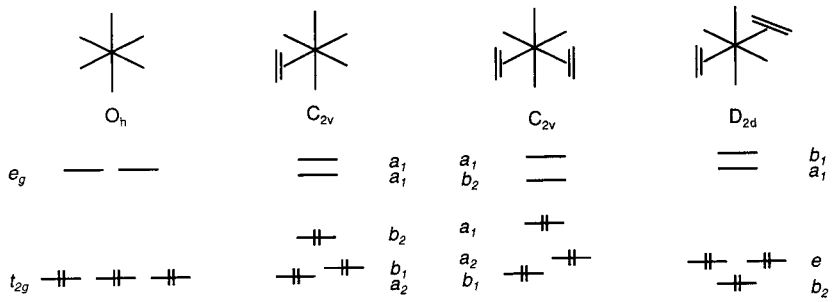

Figure 10. Qualitative d-level diagrams for $W(CO)_6$, $W(CO)_5(\eta^2$-olefin), *cis*-$W(CO)_4(\eta^2$-olefin$)_2$, and *trans*-$W(CO)_4(\eta^2$-olefin$)_2$.

the material balance was satisfactory throughout (≥90%) up to the highest conversion of the starting material (ca. 80%). The solid curves in Figure 9 represent the concentrations computed on the basis of the functional relationships, eqs 1−4, using the complete set of four quantum yields. The intermediate products **2** and **3** did not accumulate to concentrations higher than ca. 20%. Clearly, the larger ϵ values at the excitation wavelength (365 nm) of **2** (1010 L·mol^{-1}·cm^{-1}) and **3** (1540 L·mol^{-1}·cm^{-1}), compared with those of **1** (305 L·mol^{-1}·cm^{-1}) and **4** (170 L·mol^{-1}·cm^{-1}), favor the further conversion into the final product **4**, despite the decreasing quantum yields for the respective steps in the reaction sequence.

Mechanistic Aspects. The photosubstitution of CO in group 6 metal carbonyls has been known for a long time as a highly efficient process.[55,56] It was thought to involve loss of CO from the $^3T_{1g}$ ligand field excited state of $M(CO)_6$[57] as the actual photochemical step, although the notion of internal conversion from singlet to the triplet manifold has been invalidated on the basis of femtosecond transient absorption measurements.[58] Moreover, recent theoretical studies have shown that the photodissociation does not necessarily require ligand field excitation, but may also occur from a charge-transfer excited state.[59]

The olefin-substituted complexes have received much less attention in this respect so that a sound theoretical basis for a discussion of the electronic absorption spectra (Figure 3) and the excited-state reactivities is not available. Qualitative d-level diagrams (Figure 10) may nevertheless be helpful in order to rationalize the distinct differences in the long-wavelength region of the spectra. Taking into account the single-face π-acceptor character of the olefin, one can expect that the replacement of one CO group by such a ligand leads to a substantial destabilization of one of the three d(π) orbitals, labeled b_2 under C_{2v} symmetry. Further destabilization of this orbital should occur upon the introduction of a second olefin in cis position to the first one, pushing the b_2 above the a_1 level, as sketched out in a qualitative molecular orbital diagram of $W(CO)_4(\eta^2$-ethene$)_2$.[19] In either case, a low-energy ligand field transition is plausible, in accord with the appearance of the shoulder around 390−400 nm in the absorption spectra of **2** and **3** (Figure 3),[60] which is responsible for the (pale) yellow color of these two complexes. The situation is different when the second olefin is oriented trans-orthogonal to the first one. In this case, two d-levels, each interacting with one of the two olefin(π*) orbitals, are equally stabilized, probably down to almost the same energy as that in $W(CO)_6$ (**1**). On the basis of this consideration, the colorless appearance of the *trans*-$W(CO)_4(\eta^2$-olefin$)_2$ complexes is readily understood.

Scheme 8

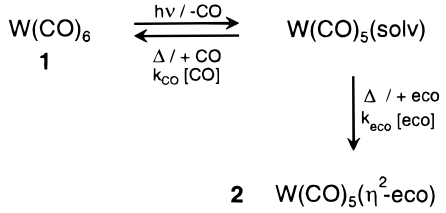

The quantum yield $\Phi_{12} = 0.73$ for the conversion of $W(CO)_6$ (**1**) into the monosubstituted olefin complex **2** is in good agreement with the previously reported value for the analogous photosubstitution of CO by pyridine as the incoming ligand ($\Phi = 0.78 \pm 0.05$, at $\lambda = 366$ nm).[56b] Hence, it seems that these data essentially represent the efficiency of the photolytic generation of the $W(CO)_5$(solv) fragment, which has been discussed in terms of a model where most of the ejected CO ligands can escape from the coordination site without leaving the solvent cage.[61] In principle, re-coordination of liberated CO, still present in the bulk solution, may compete with the formation of the olefin-substituted product **2** (Scheme 8). However, as can be estimated from the previously determined rate constants,[28,62] the reformation of **1** should be negligible since, due to the presence of *(E)*-cyclooctene in sufficiently large excess, k_{CO}[CO] ≪ k_{eco}[eco] at any stage of the conversion.

As known from the low-temperature matrix experiments, $W(CO)_5(\eta^2$-eco) (**2**) undergoes photolytic detachment of the olefin ligand and loss of CO as well, yielding

(55) (a) Strohmeier, W.; Gerlach, K. *Chem. Ber.* **1961**, *94*, 368−406. (b) Strohmeier, W.; von Hobe, D. *Chem. Ber.* **1961**, *94*, 761−765. (c) Strohmeier, W.; von Hobe, D. *Chem. Ber.* **1961**, *94*, 2031−2037. (d) Strohmeier, W.; von Hobe, D. *Z. Phys. Chem N. F.* **1962**, *34*, 393−400. (e) Kling, O.; Nikolaiski, E.; Schläfer, H. L. *Ber. Bunsen-Ges. Phys. Chem.* **1963**, *67*, 883−892. (f) Strohmeier, W. *Ber. Bunsen-Ges. Phys. Chem.* **1963**, *67*, 892−893. (g) Vogler, A. *Z. Naturforsch.* **1970**, *25b*, 1069−1070.

(56) (a) Nasielski, J.; Colas, A. *J. Organomet. Chem.* **1975**, *101*, 215−219. (b) Nasielski, J.; Colas, A. *Inorg. Chem.* **1978**, *17*, 237−240.

(57) Beach, N. A.; Gray, H. B. *J. Am. Chem. Soc.* **1968**, *90*, 5713−5721.

(58) Joly, A. G.; Nelson, K. A. *Chem. Phys.* **1991**, *152*, 69−82.

(59) (a) Pollak, C.; Rosa, A.; Baerends, E. J. *J. Am. Chem. Soc.* **1997**, *119*, 7324−7329. (b) Pierloot, K.; Tsokos, E.; Vanquickenborne, L. G. *J. Phys. Chem.* **1996**, *100*, 16545−16550.

(60) By analogy with the recent reassignment of the respective transition in $Cr(CO)_6$,[59] these features may just as well be attributed to metal d(π) → ligand(π*) charge-transfer transitions, which, however, does not disturb the essence of the argumentation.

(61) Burdett, J. K.; Grzybowski, J. M.; Perutz, R. N.; Poliakoff, M.; Turner, J. J.; Turner, R. F. *Inorg. Chem.* **1978**, *17*, 147−154.

(62) Schaffner, K.; Grevels, F.-W. *J. Mol. Struct.* **1988**, *173*, 51−65.

Scheme 9

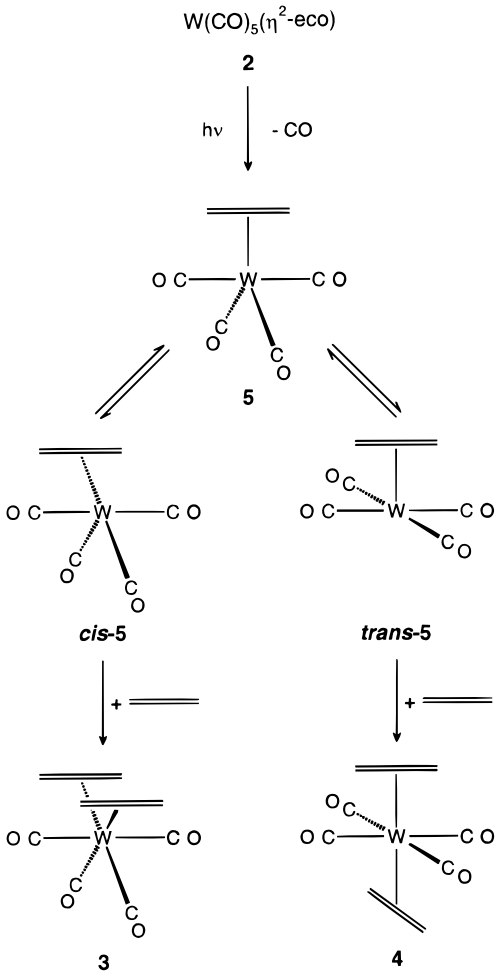

the fragments $W(CO)_5$ and $W(CO)_4(\eta^2\text{-eco})$, respectively. In solution containing an excess of *(E)*-cyclooctene, the former species is rapidly captured with regeneration of **2**. Hence it is not surprising that the quantum yield for the disappearance of **2** ($\Phi_{23} + \Phi_{24} = 0.50$) is substantially lower than Φ_{12} (0.73).

What remains to be addressed is the nature of the $W(CO)_4(\eta^2\text{-eco})$ fragment (**5**) and its possible role as a common intermediate en route to the disubstituted products **3** and **4**. In a theoretical study,[13] various geometries of the related $Mo(CO)_4(\eta^2\text{-ethene})$ have been examined. A distorted trigonal-bipyramidal structure (90° angle between the equatorial CO groups, olefin upright oriented in an equatorial position) was calculated to be the most stable one, but at the same time was thought to be less reactive toward an entering ligand compared with a square-pyramidal geometry. Hence we suggest this trigonal-bipyramidal structure for the observed fragment **5**, which moves energetically uphill on the reaction coordinate to assume a square-pyramidal geometry prior to taking up the second olefin (Scheme 9). The present knowledge does not allow the prediction of whether $W(CO)_5(\eta^2\text{-eco})$ (**2**) loses CO from a cis or trans position to the olefin. Taking into account that, according to the aforementioned theoretical study,[13] the square pyramid having the olefin situated in a basal position (*cis*-**5**, i.e., the vacant site cis to the olefin) should be lower in energy than the one with the olefin in the apical position (*trans*-**5**, i.e., the vacant site trans to the olefin),[13] one readily understands why *cis*-$W(CO)_4(\eta^2\text{-eco})_2$ (**3**) is more easily formed than *trans*-$W(CO)_4(\eta^2\text{-eco})_2$ (**4**), $\Phi_{23} = 0.34$ versus $\Phi_{24} = 0.16$.

Concrete information on the mechanism of the *cis*- → *trans*-$W(CO)_4(\eta^2\text{-eco})_2$ photoisomerization (**3** → **4**) is not yet available. Nevertheless, photolytic detachment of an olefin ligand from **3** with formation of the $W(CO)_4(\eta^2\text{-eco})$ fragment **5**, followed by competitive capturing of *cis*-**5** or *trans*-**5** by *(E)*-cyclooctene according to Scheme 9, seems to be a reasonable proposal which also accounts for the moderate quantum yield ($\Phi_{34} = 0.15$). The much lower quantum yield for the reverse reaction ($\Phi_{43} \leq 0.01$) may be due to the particularly high stability of the trans-orthogonal $M(\eta^2\text{-olefin})_2$ arrangement, which could render the (reversible) dissociation of CO from **4** a more favorable process than loss of the olefin.

Conclusion

The mechanism, elucidated in great detail for the particular case of the photochemical synthesis of *trans*-$W(CO)_4(\eta^2\text{-eco})_2$ (**4**), should be generally applicable to the conversion of group 6 metal hexacarbonyls into disubstituted *trans*-$M(CO)_4(\eta^2\text{-olefin})_2$ derivatives. It involves a *cis*-$M(CO)_4(\eta^2\text{-olefin})_2$ complex as a key intermediate en route from $M(CO)_5(\eta^2\text{-olefin})$ to the final product, while the direct trans-disubstitution is of minor importance. Hence, accumulation of *cis*-$M(CO)_4(\eta^2\text{-olefin})_2$ to a concentration sufficiently high for competitive light absorption in the reaction mixture is essential in order to render the cis → trans photoisomerization feasible. Taking into account that, in general, complexes of the type *cis*-$M(CO)_4(\eta^2\text{-olefin})_2$ are thermally labile, one can understand that the synthesis of *trans*-$Cr(CO)_4(\eta^2\text{-ethene})_2$,[2,3] for example, requires low-temperature conditions. In such cases, ambient temperature causes the photosubstitution of $Cr(CO)_6$ to stop at the stage of the monosubstituted $Cr(CO)_5(\eta^2\text{-olefin})$ complex,[4,6] which in this way can be produced on preparative scale without significant contamination, if any,[6] by the disubstituted complex. Thus, the intimate knowledge of the mechanism enables one to select the conditions for directing the reaction to the desired product.

Acknowledgment. It is our pleasure to dedicate this paper to Professor Dietrich Döpp on the occasion of his 60th birthday. S.Ö. is grateful to the Alexander von Humboldt-Stiftung for a research fellowship. The authors thank P. Bayer, C. Jäger, G. Klihm, D. Kreft, R. Schrader, and the staff of the service laboratories at the MPI für Strahlenchemie and the MPI für Kohlenforschung for their skilled experimental assistance.

Appendix

Kinetic Equations for Multistep Photochemical Reactions. Scheme A-1 represents the photochemical conversion of a starting material **A** into the products **B**, **C**, and **D** in a multistep process involving both consecutive and parallel pathways.

Scheme A-1

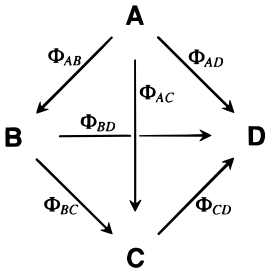

The rate expressions for the four components of the system (**A**, **B**, **C**, **D)** are given in eqs A-1 to A-4.

$$-\frac{dc_A}{dt} = (\Phi_{AB} + \Phi_{AC} + \Phi_{AD})\chi_A Q_{abs} \quad \text{(A-1)}$$

$$\frac{dc_B}{dt} = [\Phi_{AB}\chi_A - (\Phi_{BC} + \Phi_{BD})\chi_B]Q_{abs} \quad \text{(A-2)}$$

$$\frac{dc_C}{dt} = [\Phi_{AC}\chi_A + \Phi_{BC}\chi_B - \Phi_{CD}\chi_C]Q_{abs} \quad \text{(A-3)}$$

$$\frac{dc_D}{dt} = [\Phi_{AD}\chi_A + \Phi_{BD}\chi_B + \Phi_{CD}\chi_C]Q_{abs} \quad \text{(A-4)}$$

The factors χ_A, χ_B, χ_C, and χ_D are the so-called "molar fractions of light",[22c,63] which represent the portion of light absorbed by the individual compounds **A**, **B**, **C**, and **D**:

$$\chi_A = \frac{\epsilon_A c_A}{\epsilon_A c_A + \epsilon_B c_B + \epsilon_C c_C + \epsilon_D c_D} = \frac{\epsilon_A c_A}{\sum_i \epsilon_i c_i} \quad \text{etc.} \quad \text{(A-5)}$$

The light absorption rate, Q_{abs} [einstein·L^{-1}·s^{-1}], is given by

$$Q_{abs} = \frac{I_0}{l}(1 - 10^{-l\sum \epsilon_i c_i}) \quad \text{(A-6)}$$

where I_0 is the incident photon flux (which may vary with time) and l is the path length.

The integration of eqs A-1 to A-4 ultimately yields the concentrations as functions of the amount of absorbed light, thus providing the functional relationships needed to determine the quantum yields. To simplify matters, the initial concentrations of **B**, **C**, and **D** are taken as zero ($c_B^0 = c_C^0 = c_D^0 = 0$). Dividing eq A-2 by eq A-1, one obtains

$$\frac{dc_B}{dc_A} = \beta\frac{c_B}{c_A} - \frac{\Phi_{AB}}{\Phi_A} \quad \text{(A-7)}$$

where $\beta = \dfrac{\epsilon_B \Phi_B}{\epsilon_A \Phi_A}$

$$\Phi_A = \Phi_{AB} + \Phi_{AC} + \Phi_{AD}$$

$$\Phi_B = \Phi_{BC} + \Phi_{BD}$$

Integration of eq A-7, for the general case of $\beta \neq 1$, yields

$$\frac{c_B}{c_A} = q\left[\left(\frac{c_A}{c_A^0}\right)^{(\beta - 1)} - 1\right] \quad \text{(A-8)}$$

where $q = \dfrac{\Phi_{AB}}{\Phi_A(1 - \beta)}$

Dividing eq A-3 by eq A-1 and inserting eq A-8, one obtains

$$\frac{dc_C}{dc_A} = \gamma\frac{c_C}{c_A} - \beta\frac{\Phi_{BC}}{\Phi_B}\frac{c_B}{c_A} - \frac{\Phi_{AC}}{\Phi_A} \quad \text{(A-9)}$$

where $\gamma = \dfrac{\epsilon_C \Phi_{CD}}{\epsilon_A \Phi_A}$

Integration of eq A-9, for the general case of $\beta \neq 1$ and $\gamma \neq 1$, yields

$$\frac{c_C}{c_A} = r_1 + r_2\left(\frac{c_A}{c_A^0}\right)^{(\beta - 1)} + r_3\left(\frac{c_A}{c_A^0}\right)^{(\gamma - 1)} \quad \text{(A-10)}$$

where $r_1 = \dfrac{1}{(1 - \gamma)}\left[\dfrac{\beta}{(1 - \beta)}\dfrac{\Phi_{BC}}{\Phi_B}\dfrac{\Phi_{AB}}{\Phi_A} - \dfrac{\Phi_{AC}}{\Phi_A}\right]$

$$r_2 = \frac{\beta}{(1 - \beta)(\gamma - \beta)}\frac{\Phi_{BC}}{\Phi_B}\frac{\Phi_{AB}}{\Phi_A}$$

$$r_3 = \frac{1}{(1 - \gamma)}\left[\frac{\Phi_{AC}}{\Phi_A} - \frac{\beta}{(\gamma - \beta)}\frac{\Phi_{AB}}{\Phi_A}\frac{\Phi_{BC}}{\Phi_B}\right]$$

The concentration of **D** is determined by the stoichiometry condition

$$c_D = c_A^0 - c_A - c_B - c_C \quad \text{(A-11)}$$

Insertion of eqs A-8, A-10, and A-11 into eq A-1 yields a differential equation for the time dependence of c_A which can be solved by integration. In general Q_{abs} is a function of the (time-dependent) concentrations (eq A-6), the explicit consideration of which would render the integration rather complicated. However, the integration can easily be carried out for two practically important cases. Either the irradiation is performed under total absorption conditions (which renders the power term in eq A-6 negligible), or an integrating actinometer is used which provides a numerical value for the total amount of light absorbed by the system, $\int_0^t Q_{abs}\,dt$. This latter technique also eliminates any problem arising from nonconstant incident photon fluxes. For these two cases, c_A is obtained as an implicit function of the amount of absorbed light, eq A-12.

$$p_1\left[1 - \frac{c_A}{c_A^0}\right] + p_2\left[1 - \left(\frac{c_A}{c_A^0}\right)^{\beta}\right] + p_3\left[1 - \left(\frac{c_A}{c_A^0}\right)^{\gamma}\right] - \epsilon_D \ln\left(\frac{c_A}{c_A^0}\right) = \frac{\epsilon_A \Phi_A}{c_A^0}\int_0^t Q_{abs}\,dt \quad \text{(A-12)}$$

(63) Mark. G.; Mark, F. *Z. Naturforsch.* **1974**, *29a*, 610−613.

where

$$p_1 = (\epsilon_A - \epsilon_D) - \frac{(\epsilon_B - \epsilon_D)}{(1-\beta)}\frac{\Phi_{AB}}{\Phi_A} + \frac{(\epsilon_C - \epsilon_D)}{(1-\gamma)}\left[\frac{\beta}{(1-\beta)}\frac{\Phi_{BC}}{\Phi_B}\frac{\Phi_{AB}}{\Phi_A} - \frac{\Phi_{AC}}{\Phi_A}\right]$$

$$p_2 = \frac{(\epsilon_B - \epsilon_D)}{\beta(1-\beta)}\frac{\Phi_{AB}}{\Phi_A} + \frac{(\epsilon_C - \epsilon_D)}{(1-\beta)(\gamma-\beta)}\frac{\Phi_{AB}}{\Phi_A}\frac{\Phi_{BC}}{\Phi_B}$$

$$p_3 = \frac{(\epsilon_C - \epsilon_D)}{\gamma(1-\gamma)}\left[\frac{\Phi_{AC}}{\Phi_A} - \frac{\beta}{(\gamma-\beta)}\frac{\Phi_{AB}}{\Phi_A}\frac{\Phi_{BC}}{\Phi_B}\right]$$

Recall that the concentration of **A** in eq A-12 is not given as an explicit, but rather as an implicit function of the amount of absorbed light. Therefore the value of c_A has to be evaluated numerically. The concentrations of **B**, **C**, and **D** can be obtained subsequently from eqs A-8, A-10, and A-11.

The photokinetic equations for a system involving only three compounds **A**, **B**, and **C** (Scheme A-2) can be obtained in an analogous way.

Scheme A-2

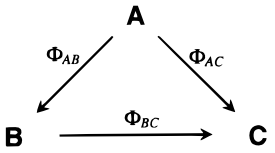

$$u_1\left[1 - \frac{c_A}{c_A^0}\right] + u_2\left[1 - \left(\frac{c_A}{c_A^0}\right)^{\beta}\right] - \epsilon_C \ln\left(\frac{c_A}{c_A^0}\right) = \frac{\epsilon_A \Phi_A}{c_A^0}\int_0^t Q_{abs}\, dt \quad \text{(A-13)}$$

$$\frac{c_B}{c_A} = q\left[\left(\frac{c_A}{c_A^0}\right)^{(\beta-1)} - 1\right] \quad \text{(A-14)}$$

$$c_C = c_A^0 - c_A - c_B \quad \text{(A-15)}$$

where $\Phi_A = \Phi_{AB} + \Phi_{AC}$

$$u_1 = (\epsilon_A - \epsilon_C) - \frac{(\epsilon_B - \epsilon_C)}{(1-\beta)}\frac{\Phi_{AB}}{\Phi_A}$$

$$u_2 = \frac{1}{\beta(1-\beta)}\frac{\Phi_{AB}}{\Phi_A}(\epsilon_B - \epsilon_C)$$

$$q = \frac{1}{1-\beta}\frac{\Phi_{AB}}{\Phi_A}$$

The photokinetic formalism outlined above can easily be extended to systems with more than four components. The concentrations of all products **B**, **C**, **D**, **E**, etc. can be expressed as functions of the concentration of the starting material **A** since the differential equations relating c_A to the concentration of any consecutive product can be integrated in closed form, beginning with **B** and proceeding stepwise to the ultimate product. Hence, in the final step the rate expression for **A** can also be integrated in closed form to yield c_A as an implicit function of the amount of absorbed light.

Treatment of Special Cases. It should be emphasized that the eqs A-8, A-10, and A-12 become singular for the special cases of $\beta = 1$ and/or $\gamma = 1$ and/or $\beta = \gamma$ and therefore require modifications. For each of the various combinations of these special cases the integration of the differential equations will give different analytical formulas. For example, for $\beta = 1$ the solution of eq A-7 takes the form $c_B/c_A = (\Phi_{AB}/\Phi_A)\ln(c_A^0/c_A)$, which is different from eq A-8. A more convenient approach, however, is to start with the equations derived for the general case (eqs A-8, A-10, and A-12) and to transform the indeterminate forms into determinate forms by applying L'Hôpital's rule once or, if necessary, twice.

Moreover, general formulas, valid for all values of β and γ, have been developed. All singularities can be removed by inserting the Taylor expansion

$$y^x = e^{x \ln y} = \sum_{\nu=0}^{\infty}\frac{1}{\nu!}(x \ln y)^{\nu} \quad \text{(A-16)}$$

into these equations and collecting those terms of the infinite sum which do not cancel into remainder functions $R^{(n)}$ and $\tilde{R}^{(n)}$. These functions are defined by

$$R^{(n)}(y,\xi) = \sum_{\nu=n}^{\infty}\xi^{\nu-1}\frac{(\ln y)^{\nu}}{\nu!} \quad \text{(A-17)}$$

and

$$\tilde{R}^{(n)}(y,\eta,\xi) = (R^{(n+1)}(y,\eta+\xi) - R^{(n+1)}(y,\eta))\frac{1}{\xi} = \sum_{\nu=n}^{\infty} g_{\nu}\frac{(\ln y)^{\nu+1}}{(\nu+1)!} \quad \text{(A-18)}$$

where

$$g_{\nu} = \frac{(\eta+\xi)^{\nu} - \eta^{\nu}}{\xi} \quad \text{and} \quad n \geq 1$$

After some algebraic manipulations the following expression is obtained from eq A-12:

$$d_1(\tilde{c}_A - 1) + d_2\tilde{c}_A R^{(1)}(\tilde{c}_A,\beta-1) + d_3\tilde{c}_A\tilde{R}^{(1)}(\tilde{c}_A,\beta-1,\gamma-\beta) + \epsilon_D \ln \tilde{c}_A + d_4(\gamma-\beta)\tilde{c}_A\tilde{R}^{(1)}(\tilde{c}_A,\beta-1,\gamma-\beta) = -\frac{\epsilon_A\Phi_A}{c_A^0}\int_0^t Q_{abs}\, dt \quad \text{(A-19)}$$

where

$$\tilde{c}_A = c_A/c_A^0, \quad \beta = (\epsilon_B\Phi_B)/(\epsilon_A\Phi_A), \quad \gamma = (\epsilon_C\Phi_{CD})/(\epsilon_A\Phi_A),$$

and

$$d_1 = (\epsilon_A - \epsilon_D) + \frac{\epsilon_B - \epsilon_D}{\beta}\frac{\Phi_{AB}}{\Phi_A} + \frac{\epsilon_C - \epsilon_D}{\gamma}\left(\frac{\Phi_{AC}}{\Phi_A} + \frac{\Phi_{AB}}{\Phi_A}\frac{\Phi_{BC}}{\Phi_B}\right)$$

$$d_2 = -\frac{\epsilon_B - \epsilon_D}{\beta}\frac{\Phi_{AB}}{\Phi_A} - \frac{\epsilon_C - \epsilon_D}{\gamma}\left(\frac{\Phi_{AC}}{\Phi_A} + \frac{\Phi_{AB}}{\Phi_A}\frac{\Phi_{BC}}{\Phi_B}\right)$$

$$d_3 = (\epsilon_C - \epsilon_D)\frac{\Phi_{AB}}{\Phi_A}\frac{\Phi_{BC}}{\Phi_B}\frac{\beta}{\gamma}$$

$$d_4 = -\frac{(\epsilon_C - \epsilon_D)}{\gamma}\frac{\Phi_{AC}}{\Phi_A}$$

Similarly, eq A-8 can be cast into the form

$$\frac{c_B}{c_A} = -\frac{\Phi_{AB}}{\Phi_A}R^{(1)}(\tilde{c}_A,\beta - 1) \qquad \text{(A-20)}$$

and eq A-10 into the form

$$\frac{c_C}{c_A} = \frac{\Phi_{AB}}{\Phi_A}\frac{\Phi_{BC}}{\Phi_B}\beta\tilde{R}^{(1)}(\tilde{c}_A,\beta - 1,\gamma - \beta) - \frac{\Phi_{AC}}{\Phi_A}R^{(1)}(\tilde{c}_A,\gamma - 1) \qquad \text{(A-21)}$$

By noting that $R^{(1)}(y,0) = \ln y$ and $\tilde{R}^{(1)}(y,0,0) = (\ln y)^2/2$, explicit formulas can be derived for the special cases from eqs A-19, A-20, and A-21. Numerical values for the remainder functions A-17 and A-18 can be conveniently calculated in a recursive way as follows. Set $T_n = \xi^{n-1}[(\ln y)^n/n!]$ and $S_n = 0$. Then, for $\nu \geq n$, calculate $S_{\nu+1} = S_\nu + T_\nu$ and update $T_{\nu+1} = T_\nu\xi[\ln y/(\nu + 1)]$ as long until $T_{\nu+1}$ becomes sufficiently small compared to $S_{\nu+1}$, such that $R^{(n)} \approx S_{\nu+1}$. Values of $\tilde{R}^{(n)}$ can be calculated in an analogous way, whereby the expansion coefficients g_ν also can be obtained recursively according to $g_{\nu+1} = (\eta + \xi)g_\nu + \eta_\nu$, starting from $g_0 = 0$.

Supporting Information Available: Tables of bond lengths and angles, atomic coordinates, and thermal parameters for $W(CO)_6$ (**1**), $W(CO)_5(\eta^2$-*(E)*-cyclooctene) (**2**), *trans*-$W(CO)_4(\eta^2$-*(E)*-cyclooctene$)_2$ (meso compound **4a** with S_4 symmetry), and *cis*-$W(CO)_4(\eta^2$-*(Z)*-cyclooctene$)_2$. This material is available free of charge via the Internet at http://pubs.acs.org.

OM990300T